# Information flow across the cortical timescales hierarchy during narrative construction

Claire H. C. Chang[1,*], Samuel A. Nastase[1,*], and Uri Hasson[1]

1. Princeton Neuroscience Institute, Princeton University, Princeton, New Jersey, 08540, USA.

* To whom correspondence should be addressed:

Claire H. C. Chang, claire.hc.chang@gmail.com; Samuel A. Nastase, sam.nastase@gmail.com

**Competing Interest Statement:** The authors declare no competing financial interests.

**Classification**: biological science, neuroscience

**Keywords**: cortical hierarchy, naturalistic stimuli, fMRI, functional connectivity, language processing

## Abstract

When listening to spoken narratives, we must integrate information over multiple, concurrent timescales, building up from words to sentences to paragraphs to a coherent narrative. Recent evidence suggests that the brain relies on a chain of hierarchically organized areas with increasing temporal receptive windows to process naturalistic narratives. We hypothesized that the structure of this cortical processing hierarchy should result in an observable sequence of response lags between networks comprising the hierarchy during narrative comprehension. This study uses functional MRI to estimate the response lags between functional networks during narrative comprehension. We use inter-subject cross-correlation analysis to capture network connectivity driven by the shared stimulus. We found a fixed temporal sequence of response lags—on the scale of several seconds—starting in early auditory areas, followed by language areas, the attention network, and lastly the default mode network. This gradient is consistent across eight distinct stories but absent in data acquired during rest or using a scrambled story stimulus, supporting our hypothesis that narrative construction gives rise to inter-network lags. Finally, we build a simple computational model for the neural dynamics underlying the construction of nested narrative features. Our simulations illustrate how the gradual accumulation of information within the boundaries of nested linguistic events, accompanied by increased activity at each level of the processing hierarchy, can give rise to the observed lag gradient.

## Significance Statement

Our findings reveal a consistent, stimulus-driven gradient of lags in connectivity along the cortical processing hierarchy—from early auditory cortex to the language network, then to the default mode network—during the comprehension of naturalistic, spoken narratives. We provide a simple computational model for the neural dynamics underlying the construction of nested narrative features, allowing us to systematically explore the conditions under which the lag gradient emerges and synthesize our results with previous findings based on simple well-controlled language stimuli. Our results illustrate the isomorphism between hierarchically structured neural dynamics and hierarchically structured, real-world narrative inputs.

## Introduction

Narratives are composed of nested elements that must be continuously integrated to construct a meaningful whole, building up from words to phrases to sentences to a coherent narrative (1). Recent evidence suggests that the human brain relies on a chain of hierarchically organized brain areas with increasing temporal receptive windows (TRWs) to process this temporally evolving, nested structure (Fig. 1A). This cortical hierarchy was first revealed by studies manipulating the temporal coherence of naturalistic narratives (2, 3). These studies reported a topography of processing timescales where early auditory areas respond reliably to rapidly-evolving acoustic features, adjacent areas along the superior temporal gyrus respond reliably to information at the word level, and nearby language areas respond reliably only to

61 coherent sentences. Finally, areas at the top of the processing hierarchy in the default
62 mode network (DMN) integrate slower-evolving semantic information over many
63 minutes (4).

64 This cortical hierarchy of increasing temporal integration windows is thought to be a
65 fundamental organizing principle of the brain (5, 6). The cortical hierarchy of TRWs in
66 humans has been described using fMRI (2, 3, 7, 8) and ECoG (9). Recent work has
67 shown that deep language models also learn a gradient or hierarchy of increasing
68 TRWs (10–12), and that manipulating the temporal coherence of narrative input to a
69 deep language model yields representations closely matching the cortical hierarchy of
70 TRWs in the human brain (13). Furthermore, the cortical hierarchy of TRWs matches
71 the intrinsic processing timescales observed during rest in humans (9, 14, 15) and
72 monkeys (16). This cortical topography also coincides with anatomical and functional
73 gradients such as long-range connectivity and local circuitry (17–19), which have been
74 shown to yield varying TRWs (20, 21).

75

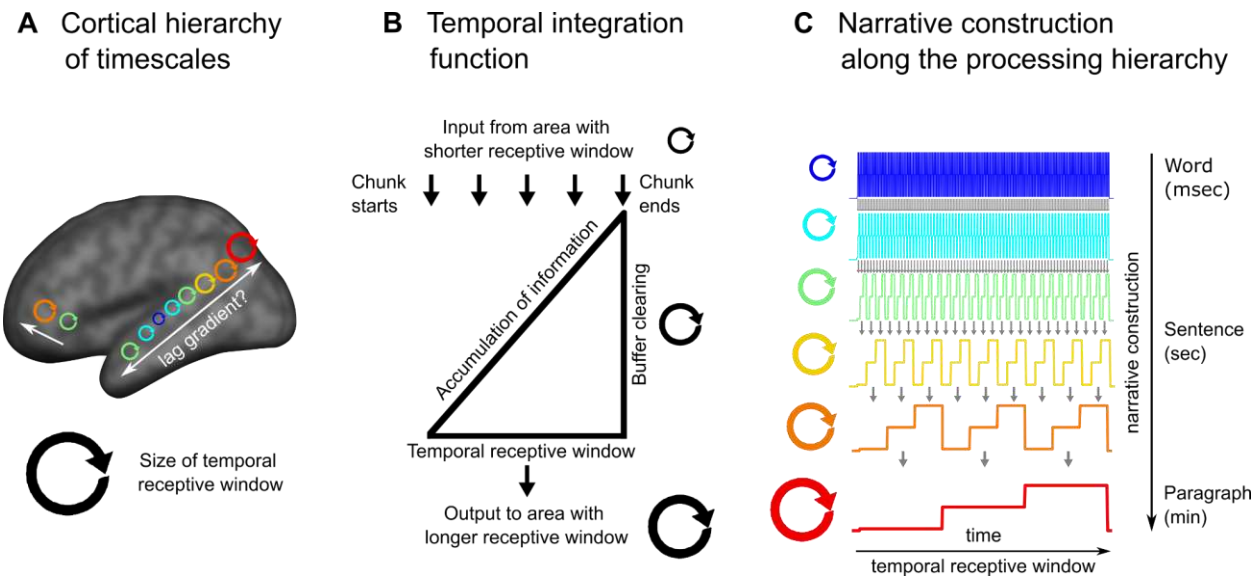


*Fig. 1. Narrative construction in the hierarchical processing framework. (A) The proposed cortical hierarchy of increasing temporal receptive windows (adapted from (5)). (B) Each level of the processing hierarchy continuously accumulates information over inputs from the preceding level. For example, phrases built over words are constructed into sentences. The accumulated information is flushed out at structural boundaries. (C) Each level of the processing hierarchy provides the building blocks for the next level, which naturally leads to longer temporal receptive windows, corresponding to linguistic units of increasing sizes. This model of narrative construction along the cortical processing hierarchy implies a gradient of response lags across the cortical hierarchy.*

The proposal that the cortex is organized according to a hierarchy of increasing TRWs implies that each area "chunks" and integrates information at its preferred temporal window and that narrative construction proceeds along the cortical hierarchy. For

example, an area that processes phrases receives information from areas that process words (Fig. 1B), which are further transmitted to areas that integrate phrases into sentences. At the end of each phrase, information is rapidly cleared to allow for real-time processing of the next phrase (1, 7). The chunking of information at varying granularity is supported by recent studies that used data-driven methods to detect boundaries as shifts between stable patterns of brain activity (22, 23).

This model of narrative construction (Fig. 1C) predicts a gradient of response lags across the cortical processing hierarchy; namely, shorter temporal lags among adjacent areas along the processing hierarchy than regions further apart in the cortical hierarchy. In the current study, we test this prediction by comparing response fluctuations elicited by spoken narratives in different brain areas using lag-correlation. We extract the lag with the peak correlation to estimate inter-region temporal difference. To focus on neural responses to linguistic and narrative information, we used inter-subject functional connectivity (ISFC) analysis (24, 25). Unlike traditional within-subject functional connectivity (WSFC), ISFC effectively filters out the idiosyncratic fluctuations that drive intrinsic functional correlations within subjects. Isolating stimulus-locked neural activity from intrinsic neural activity allows us for the first time to observe the temporal dynamics of narrative construction across the cortical hierarchy. We predicted that ISFC analysis would reveal an inter-region lag gradient during the comprehension of intact narrative, but not during scrambled-story or rest, which do not involve narrative construction. Finally, we provide a computational model to clearly illustrate how the construction of nested narrative features could give rise to the observed lag gradient, and how the lag gradient deteriorates without naturalistic inputs.

## Results

To test the hypothesis that narrative construction will yield a gradient of response lags across brain regions, we first divided the neural signals into six networks by applying k-means clustering to WSFC measured during rest (SI Appendix, Fig. S1). We labeled these networks based on anatomical correspondence with previously defined functional regions following Simony and colleagues (25), including the auditory (AUD), ventral language (vLAN), dorsal language (dLAN), default mode network (DMN), and attention (ATT) networks, aligning with the previously documented TRW hierarchy (SI Appendix, Fig. S2).

We computed lag-ISFC (i.e. cross-correlation) at varying temporal lags between all pairs of networks (Fig. 2A and SI Appendix, Fig. S3). The lags with maximum ISFC (i.e. “peak lag”) for each seed-target pair were extracted as an index for the temporal gaps in the stimulus-driven processing between each pair of networks. The extracted peak lags were color-coded to construct the network × network peak lag matrix (Fig. 2B and 2C). In the following, we describe the observed lag gradient in detail and several control analyses. Finally, we simulated the nested narrative structure and the corresponding brain responses to explore how different integration functions at different timescales could give rise to the observed lag gradient.

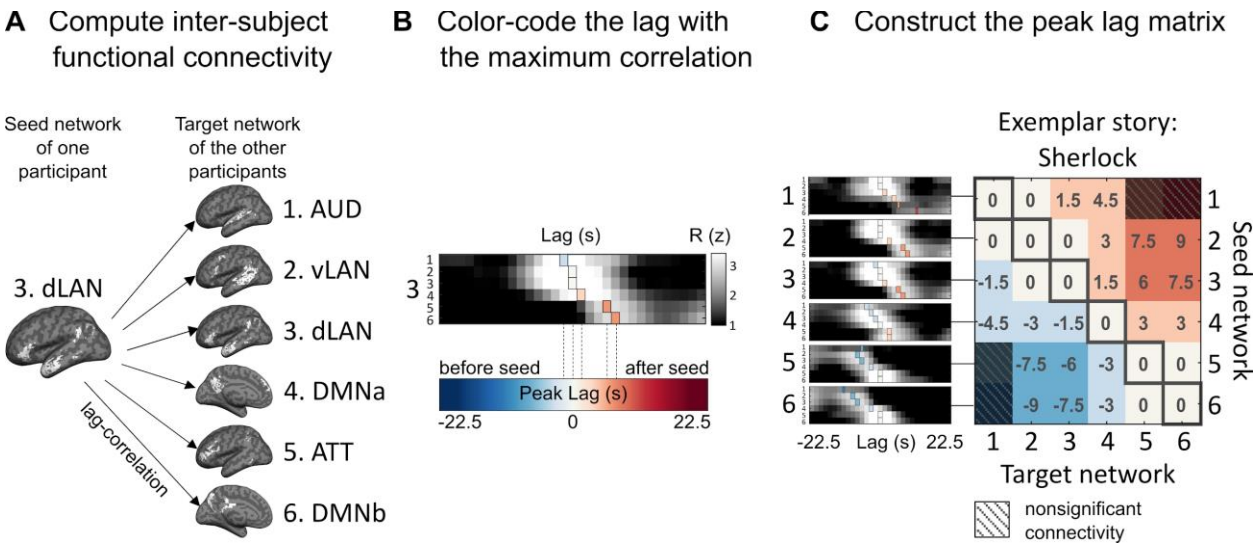


*Fig. 2. Construction of the inter-network peak lag matrix. (A) Lag-ISFC (cross-correlation) between seed-target network pairs were computed using the leave-one-subject out method. The dLAN network is used as an example seed network for illustrative purposes. (B) The matrix depicts ISFC between the dLAN seed and all six target networks at varying lags. The lag with the peak correlation value (colored vertical bars) was extracted and color-coded according to lag. For visualization, the lag-ISFCs were z-scored across lags. (C) The network × network peak lag matrix ($p < .05$, FDR corrected). Warm colors represent peak lags following the seed network, while cool colors represent peak lags preceding the seed network; zeros along the diagonal capture the intra-network ISC. An example story ("Sherlock") is shown for illustrative purposes.*

## ***Fixed lag gradient across cortical networks***

The average lag-ISFC across stories was computed for each seed network (Fig. 3A, left). The lag-ISFC between a seed network and the same network in other subjects always peaked at lag 0, reflecting the strong stimulus-locked within-network

149 synchronization reported in the ISC literature (3, 26, 27) (SI Appendix, Fig. S3).
150 Interestingly, however, non-zero peak lags were found between different networks.
151 Relative to a low-level seed, putatively higher-level networks showed peak connectivity
152 at increasing lags. For example, the stimulus-induced activity in dLAN lagged 1 TR (1.5
153 s) behind activity in AUD, whereas the activity in DMNb lagged 4 TRs (6 s) behind
154 activity in dLAN. Importantly, regardless of the choice of seed, the target networks
155 showed peak connectivity in a fixed order progressing through AUD, vLAN, dLAN,
156 DMNa, ATT, and DMNb.

157 To summarize the findings, we color-coded the peak lags and collated them into a peak
158 lag matrix where each row corresponds to a seed network and each column
159 corresponds to a target network (Fig. 3A, right; see SI Appendix, Fig. S4 for the lag-
160 ISFC waveforms). The white diagonal indicates a peak at zero lag within each area,
161 reflecting the intra-network synchronization across subjects (i.e. ISC) (SI Appendix, Fig.
162 S3), while the cool-to-warm color gradient indicates a fixed order of peak lags. For
163 example, the first row shows a white-to-warm gradient, reflecting that when AUD served
164 as the seed, other networks were either synchronized with or followed AUD, but never
165 preceded it. Conversely, the cool-to-white gradient of the last row indicates that all other
166 networks preceded the DMNb seed. The lag gradient can also be observed in individual
167 stories (SI Appendix, Fig. S5), although these patterns are noisier than the averaged
168 results. The lag gradient proceeded in a fixed order across all networks, suggesting that
169 bottom-up narrative construction is reflected in lagged connectivity between stages
170 along the cortical hierarchy from AUD up to DMNb. Similar results were obtained when
171 we defined the ROIs using the TRW hierarchy (SI Appendix, Fig. S2D).

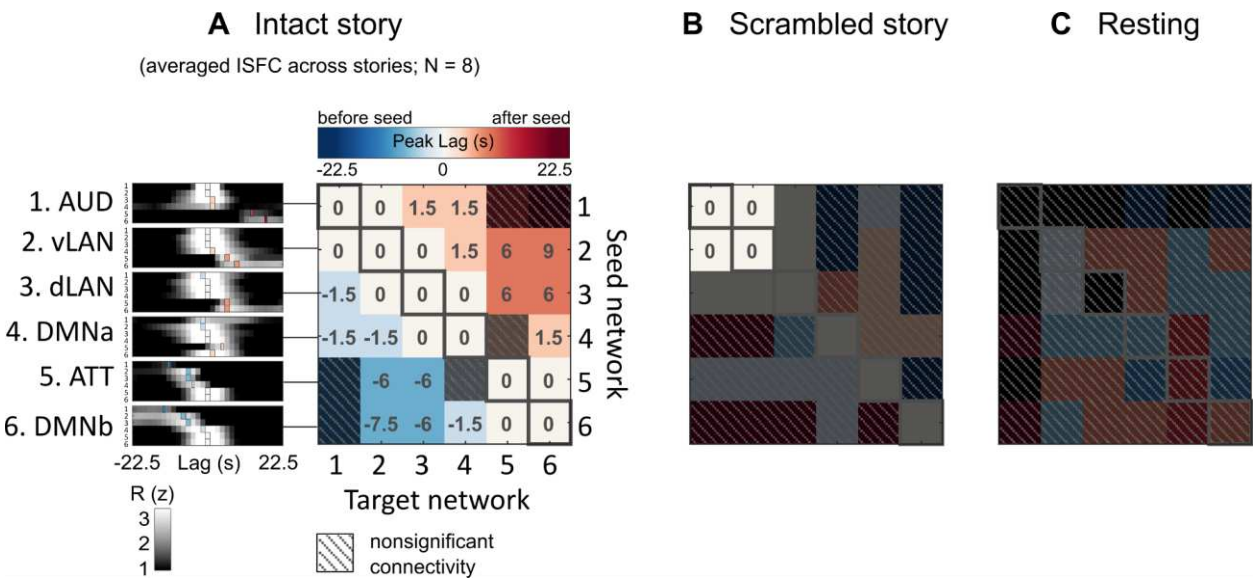


172

173 *Fig. 3. The peak lag matrix across eight stories reveals a fixed lag gradient across*
174 *networks, which is abolished during scrambled narratives and rest. (A) The network ×*
175 *network peak lag matrix is based on the averaged lag-ISFC across eight stories. For*
176 *visualization, lag-ISFC curves at left were z-scored across lags. (B) Peak lag matrix*
177 *based on responses to a scrambled story stimulus (scrambled words). (C) Peak lag*
178 *matrix based on resting-state data. Peak lag matrices are thresholded at p < .05 (FDR*
179 *corrected).*

180 ***Temporal scrambling abolishes the lag gradient***

181 We hypothesized that the lag gradient reflects the emergence of macroscopic story
182 features (e.g. narrative situations or events) integrated over longer periods of time in
183 higher-level cortical networks (22, 23). To support this point, we next used the same
184 procedure to compute the peak lag matrix for a temporally scrambled version of one
185 story ("Pie Man"; as for the results of intact "Pie Man", please see *SI Appendix, Fig. S5*).
186 In this dataset, the story stimulus was spliced at the word level and scrambled, thus

187 maintaining similar low-level sensory statistics while abolishing the slower-evolving
188 narrative content. The peak lag matrix for the scrambled story revealed synchronized
189 responses at lag 0 both within and between the AUD and vLAN networks, but no
190 significant peaks within or between other networks (Fig. 3B). This reflects low-level
191 speech processing limited to the word level and indicates that disrupting the narrative
192 structure of a story abolishes the temporal propagation of information to higher-level
193 cortical areas.

194 ***No lag gradient during rest***

195 As an additional control, we also examined whether the lag gradient observed during
196 the intact story could be detected during rest. The resting state is dominated by intrinsic
197 fluctuations and there is no external stimulus to drive synchronized brain activity across
198 subjects as well as propagation of activity across cortical areas. As expected, no
199 significant ISFC peaks were found (Fig. 3B). This provides further evidence that the
200 observed lag gradient is driven by the stimulus itself.

201 ***Idiosyncratic within-subject fluctuations obscure the lag gradient***

202 We next asked whether the inter-network lag gradient observed during spoken stories
203 can be observed using traditional WSFC. As expected, WSFC analysis revealed a
204 strong peak correlation at lag zero within each network, but also a peak correlation at
205 lag zero across all networks such that no gradient was observed (SI Appendix, Fig. S6).
206 This result supports the claim that ISFC analysis filters out intrinsic signal fluctuations
207 that propagate across brain areas, revealing the propagation of shared story information
208 across networks (24, 25). This result also verifies that intrinsic, inter-network differences

209 in hemodynamic responses cannot account for the lag gradient; otherwise, WSFC
210 should show a similar lag pattern as ISFC.

211 ***Lag gradient across fine-grained subnetworks***

212 To verify that the peak lag gradient could also be observed at a finer spatial scale, we
213 further divided each of the six networks into ten subnetworks, again by applying k-
214 means clustering to resting-state WSFC (k = 10 within each network). The peak lag
215 matrix between the sixty subnetworks was generated using the same methods as in the
216 network analysis (SI Appendix, Fig. S7A). We also visualized the brain map of lags
217 between one selected seed (posterior superior/middle temporal gyrus) and all the target
218 subnetworks (SI Appendix, Fig. S7B). Similar to the network level analysis, the peak lag
219 between the subnetworks revealed a gradient from the early auditory cortex to the
220 language network (auditory association cortex), then to the DMN.

221 ***Dominant bottom-up lag gradient across networks***

222 We adopted a method introduced by Mitra and colleagues (28) to discern whether there
223 are multiple parallel lag sequences between networks. We applied principal component
224 analysis (PCA) to the inter-network peak lag matrix (Fig. 3A) and examined the
225 cumulative variance accounted for across principal components. Our results revealed
226 that, at the coarse level of the cortical networks used here, the first principle component
227 explains 88.8% of the variance in our lag matrix (SI Appendix, Fig. S8). This suggests
228 that there is a single, unidirectional lag gradient across networks.

### *The lag gradient is not driven by transient linguistic boundary effects*

Prior work has reported that scene/situation boundaries in naturalistic stimuli elicit transient brain responses that vary across regions (29–34). To test whether this transient effect could drive the gradient observed in our lag matrix, we computed lag-ISFC after regressing out the effects of word, sentence, and paragraph boundaries in two stories with time-stamped annotations. As shown in SI Appendix, Fig. S9, the regression model successfully removed transient effects of the boundaries from the fMRI time series. Critically, however, the lag gradient remained qualitatively similar when accounting for boundaries, indicating that the observed lag gradient does not result from transient responses to linguistic boundaries in the story stimulus.

### *Reproducing the lag gradient by simulating narrative construction*

Narratives have a multi-level nested hierarchical structure (35) and are reported to elicit neural processing at increasingly long timescales along the cortical hierarchy (22, 23). To better understand how the construction of nested narrative features could give rise to the long inter-network lag gradient we observed, with up to 9-second lags, we created a simulation capturing the hierarchically nested temporal structure of real-world narratives and the corresponding hierarchy of cortical responses.

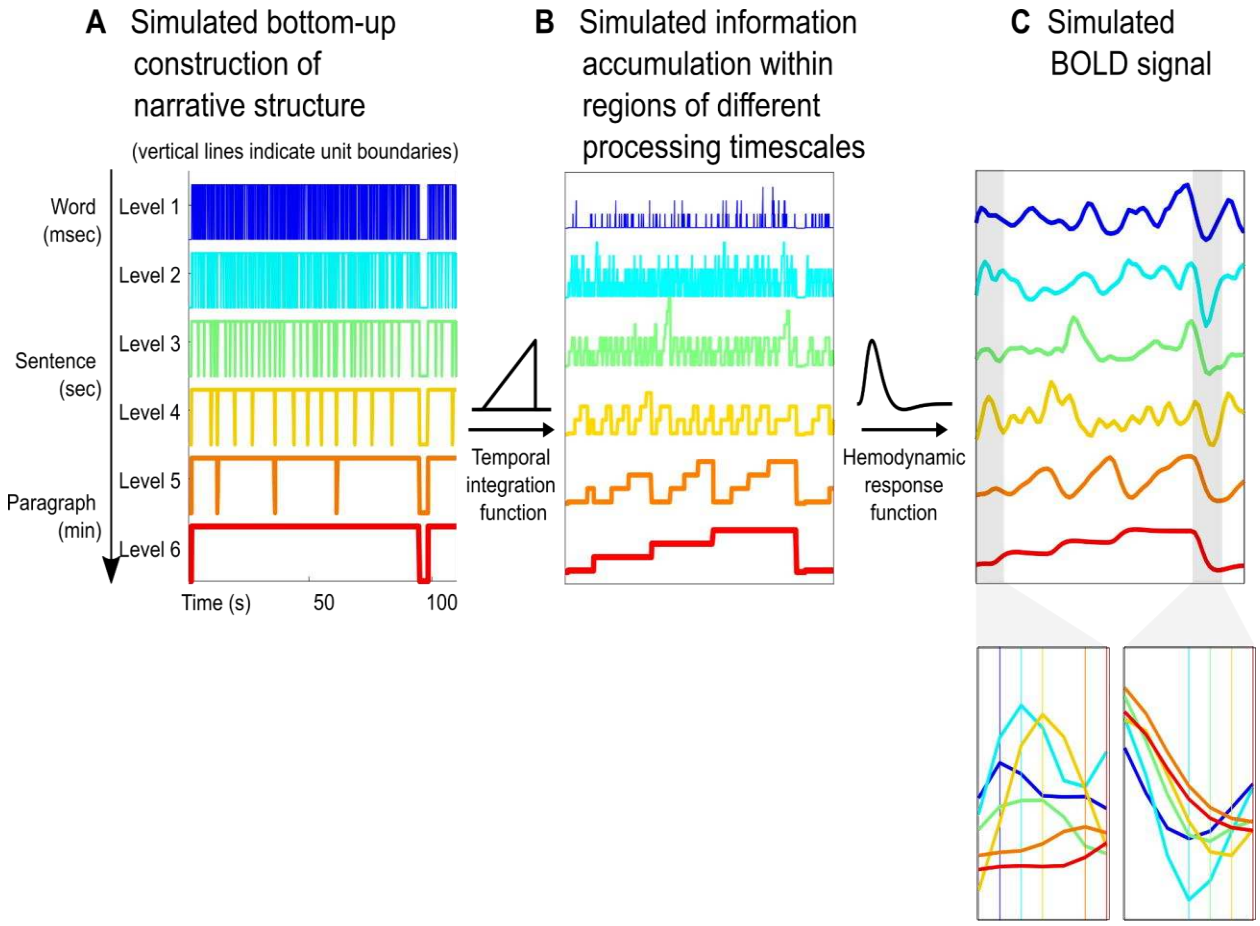


246

247 *Fig. 4. Simulating narrative construction and the corresponding brain responses. (A)*
248 *The construction of the nested narrative structure, simulated by sampling boundary*
249 *intervals from actual word durations and recursively integrating them to obtain structural*
250 *boundaries at higher levels. (B) Information accumulation at different levels is generated*
251 *by a linearly increasing temporal integration function. We postulated that information*
252 *accumulation is accompanied by increased activity. (C) BOLD responses generated by*
253 *HRF convolution. This visualization is based on parameters estimated from a spoken*
254 *story stimulus (Table S1).*

255 To match the six networks discussed so far, we simulated story features emerging
256 across six distinct timescales, which roughly correspond to words, phrases, sentences,

2–3 sentences, and paragraphs. The initial level of the simulated narrative hierarchy was populated with relatively brief low-level units, with boundary intervals sampled from actual word durations in a spoken story (SI Appendix, Fig. S10). These simulated "words" were integrated into "phrases" of varying lengths with a mean length of three words to obtain second-level boundaries (Fig. 4A). All "phrase"-level boundaries were also "word"-level boundaries. A six-level structure was ultimately generated by recursively applying this procedure. Since paragraphs are often separated in real stories by longer silent periods (SI Appendix, Fig. S11), we inserted pauses at top-level (sixth-level) boundaries. The bottom-up construction of narrative structure gives rise to inter-level alignment and increasing processing timescales at higher levels, as proposed in the hierarchical processing framework (5, 6, 18).

The simulated response amplitudes were generated using a linearly increasing temporal integration function (Fig. 4B), based on prior work showing that information accumulation is accompanied by gradually increasing activation within phrases/sentences (36–41) and paragraphs (29, 32) (a similar sentence/paragraph length effect was also observed in our data; see SI Appendix, Fig. S12). The linearly increasing temporal integration function accumulates activity derived from lower-level units within the interval between unit boundaries at the current levels and flushes out the accumulated activity at unit boundaries of the current level. To account for hemodynamic lag in the fMRI signal, we applied a canonical hemodynamic response function (HRF) to the simulated response amplitudes (Fig. 4C). We averaged the inter-level lag correlations across thirty different simulated structures (equivalent to 30

different stories) and extracted the peak lags. This peak-lag analysis parallels the analysis previously applied to the fMRI data.

The simulation allows us to systematically manipulate the narrative structure and the temporal integration function to reveal the conditions under which the lag gradient emerges. We first performed the simulation with a set of “natural” parameters roughly motivated by the temporal properties of our narrative stimuli and a simple temporal integration function reflecting linear temporal accumulation (Table S1).

This simple simulation is sufficient to reproduce the inter-network lag gradient observed in the fMRI data (Fig. 5A; as well as the ISFC at lag zero; SI Appendix, Fig. S13). In addition, we also compared the spectral properties of the simulated and real BOLD signals (SI Appendix, Fig. S14). We first computed the average power spectral density (PSD) across stories. Replicating results reported by Stephens and colleagues (15), we found stronger low-frequency fluctuations in regions with longer TRWs. Computing the PSD of the simulated brain responses similarly revealed increased low-frequency power in responses to high-level structures with longer intervals between boundaries. We then adjusted one parameter at a time to explore the parameter space constrained by natural speech.

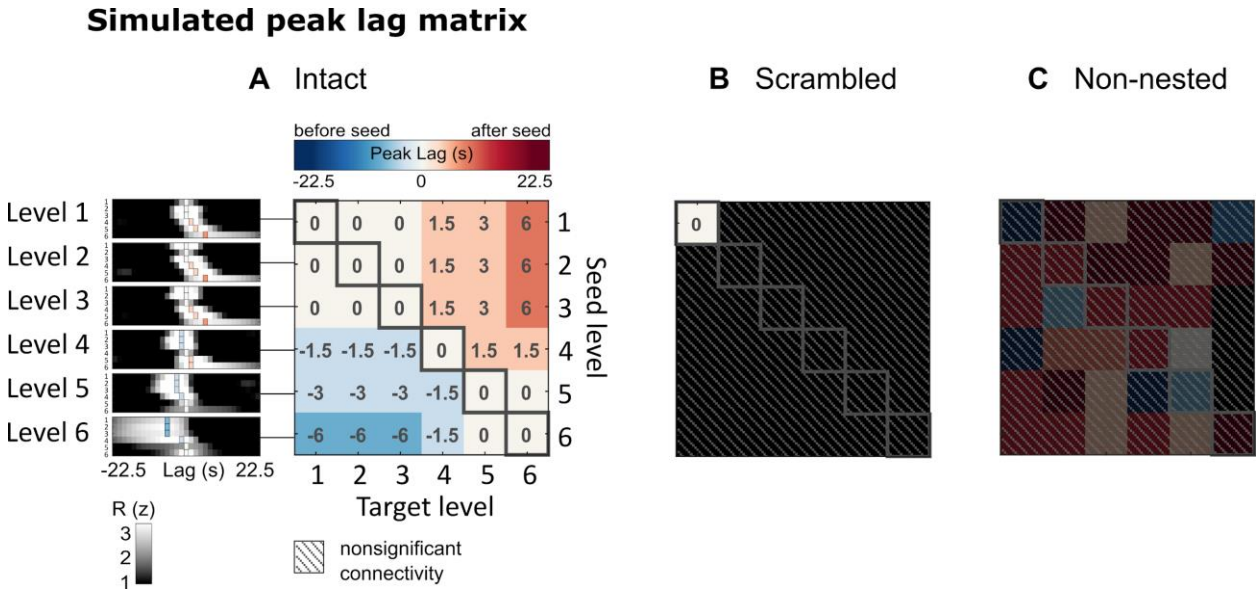


*Fig. 5. Simulated peak lag matrix. (A) Simulating the peak lag matrix observed during story-listening fMRI data (Fig. 3A) using parameters derived from a story stimulus (the same parameters as in Fig. 4 and Table S1). (B) Simulating the lag matrix observed during scrambled story (scrambled words) (Fig. 3B), by setting mean unit length = 1 and unit length variance = 0. (C) Lag matrix from the non-nested structure, created by combining levels extracted from independently generated nested structures, which disrupts the nesting relationship between different levels, similar to the scrambled story, while preserving the spectral properties of individual time series ($p < .05$, FDR correction).*

***Key parameters for the emergence of a lag gradient***

Within the bounds of natural speech (SI Appendix, Fig. S15), we observed that the simulated inter-network lag gradient is robust to varying lengths of linguistic/narrative units (mean: 2–4; variance: 0.1–1; longer length generated longer units, often with the top layers exceeding the length of the simulated story, i.e. 3000 words). The duration of

inter-paragraph pauses was estimated from two stories ("Sherlock" and "Merlin"; SI Appendix, Fig. S11) (mean length: 1.5–4.5 sec; pause effect size: 0.01–1 SD of simulated activity). We also found that the model, similar to neural responses as observed by Lerner and colleagues (42), was robust to variations in speech rate (0.5–1.5, relative to "Sherlock" speech rate). However, the lag gradient deteriorates with parameters outside of the bounds of natural speech, for example, when the inter-paragraph pause is set to 0 sec. We also simulated brain responses to word-scrambled stories by setting mean unit length = 1 and unit length variance = 0. With this setting, word-level units are never integrated into larger units (the units at each level correspond to individual words from the first level). No information integration is involved, resulting in flat activations and eliminating the difference in spectral properties of time series from different levels. No lag gradient is observed in this case (Fig. 5B).

Next, we computed inter-level lag-correlation using simulated responses to different nested structures (similar to responses to different stories), which preserves the spectral properties of individual time series while disrupting their nesting relationship. No significant lag-correlation was found when violating the nested structure of naturalistic narrative (Fig. 5C). In addition to the aforementioned linearly increasing integration function, we also explored several other temporal integration functions. We found that linearly and logarithmically increasing functions both yielded the inter-network lag gradient, but not the symmetric triangular or boxcar functions. The linearly decreasing function resulted in a reversed lag gradient (Fig. 6). These results suggest that the hierarchically nested structure that naturally arises from bottom-up narrative

334 construction and a monotonically increasing integration function are key to the
335 emergence of the lag gradient.

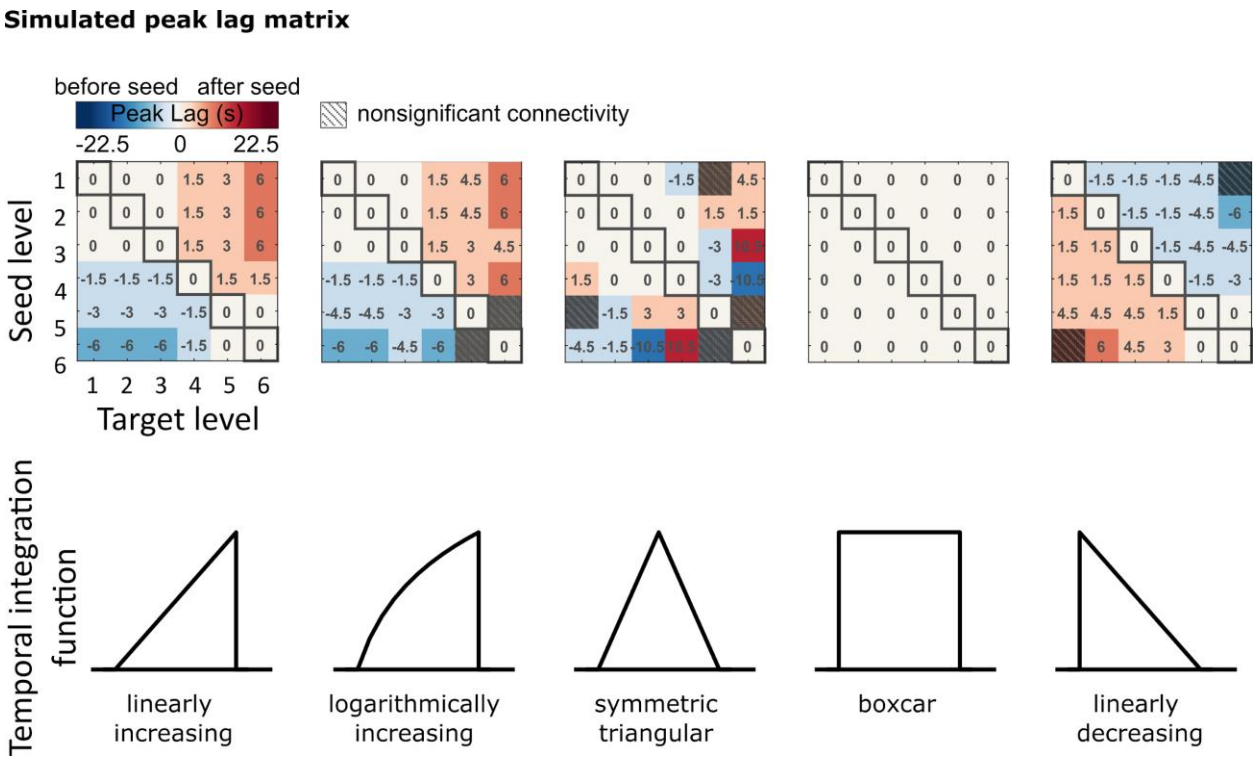


336

337 *Fig. 6. Lag matrices generated using different temporal integration functions (p < .05,*
338 *FDR correction). The linearly and logarithmically increasing temporal integration*
339 *functions yield a simulated peak lag matrix similar to the one observed in fMRI data; the*
340 *symmetric triangle and boxcar functions, as well as the linearly decreasing function, do*
341 *not.*

342

343 ## Discussion

344 By applying lag-ISFC to a collection of fMRI datasets acquired while subjects listened to
345 spoken stories, we revealed a temporal progression of story-driven brain activity along a

346 cortical hierarchy for narrative comprehension (Fig. 3A). The temporal cascade of
347 cortical responses summarized by the inter-network lag gradient was consistent across
348 stories as well as at coarse- and fine-grained functional network definitions (SI
349 Appendix, Fig. S7). The results are in line with the hierarchical processing framework,
350 which proposes a gradual emergence of narrative features of increasing duration and
351 complexity along the processing hierarchy, from early sensory areas into higher-order
352 cortical areas (Fig. 1). In support of our interpretation, we found that the lag gradient is
353 absent during rest when there is no stimulus-evoked processing (Fig. 3B), and also
354 when the temporal structure of the story is disrupted due to word scrambling (Fig. 3C).

355 We observed inter-network lags on the scale of several seconds (up to 9 seconds),
356 reflecting the temporal structure of real-world narratives, which integrate sounds into
357 words, sentences, and ideas over many seconds. Such long lags cannot be explained
358 by regional variations in neurovascular coupling (43) or transient activity impulses at
359 event boundaries. If the lag gradient only reflects variations in neurovascular coupling
360 across regions, it should be present both when we isolate stimulus-driven activity using
361 ISFC and when we examine idiosyncratic neural responses using WSFC. Instead,
362 however, the lag gradient was detected only with ISFC, but not WSFC (SI Appendix,
363 Fig. S6). Furthermore, differences in the hemodynamic response function across brain
364 areas are usually reported at shorter timescales (e.g. ~1–2 seconds) (44, 45) than the
365 0–9-second inter-network lag differences observed here in the context of narrative
366 comprehension (Fig. 3). In addition, we found that transient event boundaries (29–34)
367 did not account for the lag gradient (SI Appendix, Fig. S9).

Our simulation illustrates how narrative construction can give rise to the inter-network lag gradient by identifying three necessary conditions: (a) a cortical hierarchy of increasing processing timescales (Fig. 1 & Fig. 4) (5); (b) hierarchically nested linguistic/narrative events of increasing size along the processing hierarchy (Fig. 5B & 5C) (22, 23); and (c) gradual increasing brain activity, along with information accumulation, within the boundaries of events at each processing level (29, 32, 36–41), combined with a reset of activity (buffer clearing) at event boundaries (7) (see temporal integration function in Fig. 1B and Fig. 6). In this simple model, information integration at varying granularity (e.g. word, sentence, and paragraph) is sufficient to yield the inter-network lag gradient (Fig. 5) and spectral properties observed in the fMRI data (SI Appendix, Fig. S14). Minor adjustments to other parameters within the bounds of natural speech (i.e. speech rate, silent pause, and length of linguistic/narrative unit) did not change the gradient pattern (SI Appendix, Fig. S15).

The simulation provides a simple model which bridges the discovery of TRWs using natural stimuli (2, 42) and the accumulation of activity within linguistic units found using simple, well-controlled stimuli (e.g. sentences with similar structures) (36–41). Importantly, we note that our model is not the only one that could generate the predicted lag gradient. Our aim is to combine separate findings that point to the same cortical hierarchy with the simplest model possible. In addition, narrative processing is unlikely to be purely unidirectional (46). The lag gradient only captures the dominant process of bottom-up narrative construction (SI Appendix, Fig. S8). More studies are needed to examine recurrent or bidirectional connectivity, causal relations between networks, and nonstationary information flow over time.

Our results are also consistent with reports on the spatiotemporal dynamics of brain responses to naturalistic stimuli. A hierarchically nested spatial activation pattern has been revealed using movie, spoken story, and music stimuli (22, 23, 47). Chien and colleagues (7) reported a gradual alignment of context-specific spatial activation patterns, which was rapidly flushed at event boundaries, similar to the temporal integration function we adopted here. Taken together, the empirical findings, combined with our simulation, indicate that the spatiotemporal neural dynamics reflect the structure of naturalistic, ecologically-relevant inputs (6) and that such information is preserved even with the poor temporal resolution of fMRI. Although the current findings are derived from listener-listener coupling, the inter-regional dynamics may shed light on the lags observed in speaking-listener coupling (48–53). Given a particular seed region in the speaker's brain, we would expect to observe coupling at differing lags for different target regions in the listener's brain, and these lags may vary based on the temporal structure of the speaker's narrative.

Our results demonstrate both the importance of using inter-subject methods to isolate stimulus-driven signals and the value of data aggregation. The fact that we obtained non-zero inter-network lag only with ISFC but not WSFC (SI Appendix, Fig. S6) indicates that stimulus-driven network configuration may be masked by the idiosyncratic fluctuations that dominate WSFC analyses (24, 25). Furthermore, although the inter-network lags could be observed within individual stories (SI Appendix, Fig. S5), the gradient pattern is much clearer after aggregating across stories (Fig. 3). Data aggregation is particularly important when using naturalistic stimuli because it is impossible to control the structure of each narrative (e.g. speaking style, duration,

414 complexity, and content) (35, 54–56, 56). With these methods, we are able to reveal the
415 inter-network lag gradient driven by naturalistic narratives, as predicted by the model
416 shared information flow along the cortical processing hierarchy. Further work will be
417 needed to examine recurrent or bidirectional information flow and to decode the content
418 of narrative representations—specific to each story—as they are transformed along the
419 cortical hierarchy.

420

421 ## Materials and Methods

422 ***fMRI datasets***

423 This study relied on eight openly available spoken story datasets. Seven datasets were
424 used from the "Narratives" collection (OpenNeuro:
425 https://openneuro.org/datasets/ds002245) (57), including “Sherlock” and “Merlin” (18
426 participants, 11 females) (52), “The 21st year” (25 participants, 14 females) (58), “Pie
427 Man (PNI)”, “I Knew You Were Black”, “The Man Who Forgot Ray Bradbury”, and
428 “Running from the Bronx (PNI)” (48 participants, 34 females). One dataset was used
429 from Princeton Dataspace: “Pie Man” (36 participants, 25 females)
430 (https://dataspace.princeton.edu/jspui/handle/88435/dsp015d86p269k) (25).

431 Two non-story datasets were also included as controls: a word-scrambled “Pie Man”
432 (36, participants, 20 females) dataset and a resting-state dataset (36 participants, 15
433 females) (see the Princeton DataSpace URL above) (25).

All participants reported fluency in English and were 18–40 years in age. The criteria of participant exclusion have been described in previous studies for "Sherlock", "Merlin", "The 21st year", and "Pie Man." For "Pie Man (PNI)", "I Knew You Were Black", "The Man Who Forgot Ray Bradbury", and "Running from the Bronx (PNI)," participants with comprehension scores 1.5 standard deviations lower than the group means were excluded. One participant was excluded from "Pie Man (PNI)" for excessive movement (translation along the z-axis exceeding 3 mm).

All participants provided informed, written consent, and the experimental protocol was approved by the institutional review board of Princeton University.

***fMRI preprocessing***

fMRI data were preprocessed using FSL (https://fsl.fmrib.ox.ac.uk/), including slice time correction, motion correction, and high-pass filtering (140 s cutoff). All data were aligned to standard 3 × 3 × 4 mm Montreal Neurological Institute space (MNI152). A gray matter mask was applied.

***Functional networks***

Following Simony and colleagues (25), we defined 6 intrinsic connectivity networks within regions showing reliable responses to spoken stories. Voxels showing top 30% ISC in at least 6 out of the 8 stories were included. Using the k-means method (L1 distance measure), these voxels were clustered according to their group-averaged within-subject functional connectivity with all the voxels during resting. We refer to these functional networks as the auditory (AUD), ventral language (vLAN), dorsal language (dLAN), attention (ATT), and default mode (DMNa and DMNb) networks (SI Appendix,

Fig. S1A). To ensure that our results hold for finer-grained functional networks, we further divided each of the six networks into ten subnetworks, again by applying k-means clustering to resting-state WSFC (k=10 within each superordinate network).

To compare these intrinsic functional networks to the TRW hierarchy, we computed the TRW index (i.e. intact > word-scrambled story ISC) following (8) for voxels within regions showing reliable responses to spoken stories, using the intact and word-scrambled Pie Man. Six TRW networks were then generated by splitting the TRW indices into six bins by five quantiles (SI Appendix, Fig. S2).

***WSFC, ISFC, and ISC***

In this study, within-subject functional connectivity (WSFC) refers to within-subject inter-region correlation, while inter-subject functional connectivity (ISFC) refers to inter-subject inter-region correlation. Inter-subject correlation (ISC) refers to a subset of ISFC, namely, ISFC between homologous regions (SI Appendix, Fig. S3). ISFC and ISC were computed using the leave-one-subject-out method, i.e. correlation between the time series from each subject and the average time series of all the other subjects (24).

Before computing the correlation, the first 25 and last 20 volumes of fMRI data were discarded to remove large signal fluctuations at the beginning and end of time course due to signal stabilization and stimulus onset/offset. We then averaged voxelwise time series across voxels within network/region masks and z-scored the resulting time series.

Lag-correlations were computed by circularly shifting the time series such that the non-overlapping edge of the shifted time series was concatenated to the beginning or end. The left-out subject was shifted while the average time series of the other subjects remained stationary. Fisher's z transformation was applied to the resulting correlation values prior to further statistical analysis.

***ISFC lag matrix***

We computed the network × network × lag-ISFC matrix (SI Appendix, Fig. S3) and extracted the lag with peak ISFC (correlation) value for each network pair (Fig. 2). The peak ISFC value was defined as the maximal ISFC value within the window of lags from -15 to +15 TRs; we required that the peak ISFC be larger than the absolute value of any negative peak and excluded any peaks occurring at the edge of the window.

To obtain the mean ISFC across stories, we applied two statistical tests. Only ISFC that passed both tests were considered significant. First, we performed a parametric one-tailed one-sample t-test to compare the mean ISFC against zero (N = 8 stories) and corrected for multiple comparisons by controlling the false discovery rate (FDR; (59); 6 seed × 6 target × 31 lags; $q < .05$).

Second, to exclude ISFC peaks that only reflected shared spectral properties, we generated surrogates with the same mean and autocorrelation as the original time series by time-shifting and time-reversing. We computed the correlation between the original seed and time-reversed target with time-shifts of -100 to +100 TRs. The resulting ISFC values were averaged across stories and served as a null distribution. A one-tailed z-test was applied to compare ISFCs within the window of lag -15 to +15 TRs

against this null distribution. The FDR method was used to control for multiple comparisons (seed × target × lags; $q < .05$). When assessing ISFC for each story, only this second test was applied and all possible time-shifts were used to generate the null distribution.

***Principal component analysis of the lag matrix***

We examined whether multiple lag sequences similarly contributed to the lag matrix, using the method introduced by Mitra and colleagues (28). We applied PCA to the lag matrix obtained from the averaged ISFC across stories, after transposing the matrix and zero-centering each column. Each principal component represents a pattern of relative lags, in other words, lag sequences. We computed the proportion of overall variance in the lag matrix accounted for by each component in order to determine whether more than one component played an important role.

***Word/sentence/paragraph boundary effect***

To test the transient effect of linguistic boundaries on inter-network lag, we computed the lag-ISFC after regressing out activity impulses at boundaries. A multiple regression model was built for each subject. The dependent variable was the averaged time series of each network, removing the first 25 scans and the last 20 scans as in the ISFC analysis. The regressors included an intercept, the audio envelope, and three sets of finite impulse functions (-5 to +15 TRs relative to boundary onset), corresponding to word, sentence, and paragraph (event) boundaries. We then recomputed lag-ISFC based on the residuals of the regression model.

### *Word/sentence/paragraph length effect*

We replicated the sentence length (36–41) and paragraph length (29, 32) effect with the "Sherlock" and "Merlin" datasets, which were collected from the same group of participants. The onsets and offsets of each word, sentence, and paragraph (event) were manually time-stamped. Given the low temporal resolution of fMRI (TR = 1.5 sec) and the difficulty of labeling the onset/offset of each syllable, they were estimated by dividing the duration of each word by the number of syllables it contains.

We built individual GLM models that included regressors corresponding to the presence of syllable, word, sentence, and paragraph respectively, accompanied by three parametric modulators: accumulated syllable number within words, accumulated word number within sentences, and accumulated sentence number within paragraphs. These parametric regressors were included to test whether brain activations accumulate toward the end of word/sentence/paragraph; the longer the word/sentence/paragraph the stronger the activations. In addition to the regressors of interest, one regressor was included for speech segments without clear paragraph labels. We did not orthogonalize the regressors to each other.

Effect maps of the three parametric modulators (i.e. word length, sentence length, and paragraph length) from the individual level models of both stories were smoothed with a Gaussian kernel (FWHM = 8 mm) and input to three group-level models to test the word, sentence, and paragraph length effects respectively (flexible factorial design including the main effects of story and participant; $p < .005$, not corrected). We observed sentence and paragraph length effects. Using the same threshold, no word length effect was observed,

### *Power-spectral density analysis*

We performed spectral analyses following (15). We estimated the power spectrum of the primary auditory area and a DMN area (precuneus). As for the connectivity analysis, we cropped the first 25 and last 20 scans and z-scored the time series. For each story, the resulting time series were averaged across subjects and normalized across time. The power spectrum of the group-mean time series was estimated using Welch's method with a Hamming window of width 99 sec (66 TRs) and 50% overlap (based on the parameters from (15)). The power spectra of individual voxels were averaged within the anatomical masks of left Heschl's gyrus and left precuneus from the AAL atlas. The mean spectra across stories were then computed.

### *Simulating the construction of nested narrative structures and the corresponding BOLD responses*

To illustrate how information accumulation at different timescales could account for the inter-network lag gradient during story-listening, we simulated the construction of nested narrative structures closely following the statistical structure of real spoken stories and generated BOLD responses at each processing level. To build the first level of a nested structure, we sampled a sequence of 3000 word durations with replacement from "Sherlock," which is the longest example of spontaneous speech among our datasets, recorded from a non-professional speaker without rehearsal or script (SI Appendix, Fig. S10). Boundaries between units at the first level were set up accordingly.

#### *Unit length*

First-level units were integrated into units of the next level with a lognormal distributed unit length; e.g. integrating three words into a phrase (unit length = 3) (SI Appendix, Fig.

S10). Boundaries between second-level units were inserted accordingly. Second-level units were integrated into the third-level units following the same method. A nested structure of six levels was thus generated.

*Temporal integration function*

Postulating that information accumulation is accompanied by increased activity, brain responses within each level of the nested structure were generated as a function of unit length. For example, a linear temporal integration function generates activity [1 2 3] for a “phrase" (i.e. a Level 2 unit) consisting of three "words" (i.e. Level 1 units). The first (word) level integration was computed based on syllable numbers sampled from “Sherlock” along with word durations.

*Pause length and pause effect size*

In naturalistic narratives, boundaries between high-level units are often accompanied by silent pauses (SI Appendix, Fig. S11). Therefore, we inserted pauses with normally distributed lengths at the boundaries of the highest level units (SI Appendix, Fig. S10). Activity during the pause period was set as 0.1 standard deviations below the minimum activity of each level.

To account for HRF delay in fMRI signals, we applied the canonical hemodynamic response function provided by the software SPM (https://www.fil.ion.ucl.ac.uk/spm/) (60) and resampled the output time series from a temporal resolution of 0.001 sec to 1.5 sec to match the TR in our data. We ran 30 simulations for each set of simulation parameters. Each simulation produced different narrative structures (equivalent to

different stories). The peak lag of the mean inter-level correlation across simulations was extracted and thresholded using the same method as in the ISFC analysis (Fig. 2).

To examine whether the simulated and real fMRI signals shared similar power spectra, we also applied the power-spectral density analysis to the simulated BOLD responses at each of the six levels and averaged across thirty simulations.

We started with a set of reasonable parameters (SI Appendix, Table 1) (speech rate = 1, relative to “Sherlock”; unit length mean = 3; unit length variance = 0.5; temporal integration function = linearly increasing; mean pause length = 3 sec; pause effect size = 0.1 SD of the simulated activity) and explored alternative parameter sets within the bound of natural speech to test whether inter-level lag was robust to parameter changes.

## Data availability

This study relied on eight openly available spoken story datasets. Seven datasets were used from the "Narratives" collection (OpenNeuro: https://openneuro.org/datasets/ds002245) (57), One dataset was used from Princeton Dataspace: “Pie Man” (36 participants, 25 females) (https://dataspace.princeton.edu/jspui/handle/88435/dsp015d86p269k) (25).

## Acknowledgment

This study is supported by the National Institute of Mental Health (R01-MH112357 and DP1-HD091948).

# References


1. M. H. Christiansen, N. Chater, The Now-or-Never bottleneck: A fundamental constraint on language. *Behav. Brain Sci.* **39** (2015).
2. U. Hasson, E. Yang, I. Vallines, D. J. Heeger, N. Rubin, A hierarchy of temporal receptive windows in human cortex. *J. Neurosci.* **28**, 2539–2550 (2008).
3. Y. Lerner, C. J. Honey, L. J. Silbert, U. Hasson, Topographic mapping of a hierarchy of temporal receptive windows using a narrated story. *J. Neurosci.* **31**, 2906–2915 (2011).
4. Y. Yeshurun, M. Nguyen, U. Hasson, The default mode network: where the idiosyncratic self meets the shared social world. *Nat. Rev. Neurosci.* **22**, 181–192 (2021).
5. U. Hasson, J. Chen, C. J. Honey, Hierarchical process memory: Memory as an integral component of information processing. *Trends Cogn. Sci.* **19**, 304–313 (2015).
6. S. J. Kiebel, J. Daunizeau, K. J. Friston, A hierarchy of time-scales and the brain. *PLoS Comput. Biol.* **4**, e1000209 (2008).
7. H. Y. S. Chien, C. J. Honey, Constructing and forgetting temporal context in the human cerebral cortex. *Neuron* **106**, 675-686.e11 (2020).
8. Y. Yeshurun, M. Nguyen, U. Hasson, Amplification of local changes along the timescale processing hierarchy. *Proc. Natl. Acad. Sci.*, 201701652 (2017).
9. C. J. Honey, *et al.*, Slow cortical dynamics and the accumulation of information over long timescales. *Neuron* **76**, 423–434 (2012).
10. M. E. Peters, M. Neumann, L. Zettlemoyer, W. T. Yih, Dissecting contextual word embeddings: Architecture and representation. *Proc. 2018 Conf. Empir. Methods Nat. Lang. Process. EMNLP 2018*, 1499–1509 (2018).
11. J. Vig, Y. Belinkov, Analyzing the structure of attention in a transformer language model. *Proc. 2019 ACL Workshop BlackboxNLP Anal. Interpret. Neural Netw. NLP*, 63–76 (2019).
12. P. F. Dominey, Narrative event segmentation in the cortical reservoir. *PLOS Comput. Biol.* **17**, e1008993–e1008993 (2021).
13. C. Caucheteux, A. Gramfort, J.-R. King, Model-based analysis of brain activity reveals the hierarchy of language in 305 subjects in *Conference on Empirical Methods in Natural Language Processing*, (2021).
14. R. V. Raut, A. Z. Snyder, M. E. Raichle, Hierarchical dynamics as a macroscopic organizing principle of the human brain. *Proc. Natl. Acad. Sci.* **117**, 20890–20897 (2020).
15. G. J. Stephens, C. J. Honey, U. Hasson, A place for time: The spatiotemporal structure of neural dynamics during natural audition. *J. Neurophysiol.* **110**, 2019–2026 (2013).
16. J. D. Murray, *et al.*, A hierarchy of intrinsic timescales across primate cortex. *Nat. Neurosci.* **17**, 1661–1663 (2014).

17. A. T. Baria, *et al.*, Linking human brain local activity fluctuations to structural and functional network architectures. *NeuroImage* **73**, 144–155 (2013).
18. J.-P. Changeux, A. Goulas, C. C. Hilgetag, A connectomic hypothesis for the hominization of the brain. *Cereb. Cortex*, 1–25 (2020).
19. J. M. Huntenburg, P. L. Bazin, D. S. Margulies, Large-scale gradients in human cortical organization. *Trends Cogn. Sci.* **22**, 21–31 (2018).
20. R. Chaudhuri, K. Knoblauch, M. A. Gariel, H. Kennedy, X.-J. Wang, A large-scale circuit mechanism for hierarchical dynamical processing in the primate cortex. *Neuron* **88**, 419–431 (2015).
21. M. Demirtaş, *et al.*, Hierarchical heterogeneity across human cortex shapes large-scale neural dynamics. *Neuron* **101**, 1181-1194.e13 (2019).
22. C. Baldassano, *et al.*, Discovering event structure in continuous narrative perception and memory. *Neuron* **95**, 709-721.e5 (2017).
23. L. Geerligs, M. van Gerven, K. L. Campbell, U. Güçlü, A nested cortical hierarchy of neural states underlies event segmentation in the human brain. *bioRxiv*, 2021.02.05.429165 (2021).
24. S. A. Nastase, V. Gazzola, U. Hasson, C. Keysers, Measuring shared responses across subjects using intersubject correlation. *Soc. Cogn. Affect. Neurosci.* **14**, 667–685 (2019).
25. E. Simony, *et al.*, Dynamic reconfiguration of the default mode network during narrative comprehension. *Nat. Commun.* **7**, 12141 (2016).
26. U. Hasson, Y. Nir, I. Levy, G. Fuhrmann, R. Malach, Intersubject synchronization of cortical activity during natural vision. *Science* **303**, 1634–1640 (2004).
27. J. P. Kauppi, I. P. Jääskeläinen, M. Sams, J. Tohka, Inter-subject correlation of brain hemodynamic responses during watching a movie: Localization in space and frequency. *Front. Neuroinformatics* **4**, 5 (2010).
28. A. Mitra, A. Z. Snyder, T. Blazey, M. E. Raichle, Lag threads organize the brain's intrinsic activity. *Proc. Natl. Acad. Sci. U. S. A.* **112**, E7307 (2015).
29. Y. Ezzyat, L. Davachi, What constitutes an episode in episodic memory? *Psychol. Sci.* **22**, 243–252 (2011).
30. N. K. Speer, J. M. Zacks, J. R. Reynolds, Human brain activity time-locked to narrative event boundaries. *Psychol. Sci.* **18**, 449–455 (2007).
31. C. Whitney, *et al.*, Neural correlates of narrative shifts during auditory story comprehension. *NeuroImage* **47**, 360–366 (2009).
32. T. Yarkoni, N. K. Speer, J. M. Zacks, Neural substrates of narrative comprehension and memory. *NeuroImage* **41**, 1408–1425 (2008).
33. J. M. Zacks, *et al.*, Human brain activity time-locked to perceptual event boundaries. *Nat. Neurosci.* **4**, 651–655 (2001).
34. J. M. Zacks, N. K. Speer, K. M. Swallow, C. J. Maley, The brain's cutting-room floor: Segmentation of narrative cinema. *Front. Hum. Neurosci.* **4**, 1–15 (2010).
35. R. M. Willems, S. A. Nastase, B. Milivojevic, Narratives for neuroscience. *Trends Neurosci.* **43**, 271–273 (2020).

36. C. H. C. Chang, S. Dehaene, D. H. Wu, W. J. Kuo, C. Pallier, Cortical encoding of linguistic constituent with and without morphosyntactic cues. *Cortex* **129**, 281–295 (2020).
37. E. Fedorenko, *et al.*, Neural correlate of the construction of sentence meaning. *Proc. Natl. Acad. Sci.* **113**, E6256–E6262 (2016).
38. L. Giglio, M. Ostarek, K. Weber, P. Hagoort, Commonalities and asymmetries in the neurobiological infrastructure for language production and comprehension. *Cereb. Cortex* (2021) https:/doi.org/10.1093/cercor/bhab287.
39. W. Matchin, C. Hammerly, E. Lau, The role of the IFG and pSTS in syntactic prediction: Evidence from a parametric study of hierarchical structure in fMRI. *Cortex* **88**, 106–123 (2017).
40. M. J. Nelson, *et al.*, Neurophysiological dynamics of phrase-structure building during sentence processing. *Proc. Natl. Acad. Sci. U. S. A.* **114**, E3669–E3678 (2017).
41. C. Pallier, A.-D. A. Devauchelle, S. Dehaene, Cortical representation of the constituent structure of sentences. *Proc. …* **108**, 2522–2527 (2011).
42. Y. Lerner, C. J. Honey, M. Katkov, U. Hasson, Temporal scaling of neural responses to compressed and dilated natural speech. *J. Neurophysiol.* **111**, 2433–2444 (2014).
43. D. Rangaprakash, G. R. Wu, D. Marinazzo, X. Hu, G. Deshpande, Hemodynamic response function (HRF) variability confounds resting-state fMRI functional connectivity. *Magn. Reson. Med.* **80**, 1697–1713 (2018).
44. M. G. Bright, D. P. Bulte, P. Jezzard, J. H. Duyn, Characterization of regional heterogeneity in cerebrovascular reactivity dynamics using novel hypocapnia task and BOLD fMRI. *NeuroImage* **48**, 166–175 (2009).
45. D. A. Handwerker, J. M. Ollinger, M. D'Esposito, Variation of BOLD hemodynamic responses across subjects and brain regions and their effects on statistical analyses. *NeuroImage* **21**, 1639–1651 (2004).
46. M. J. Pickering, C. Gambi, Predicting while comprehending language: A theory and review. *Psychol. Bull.* **144**, 1002–1044 (2018).
47. J. A. Williams, *et al.*, High-order areas and auditory cortex both represent the high-level event structure of music. *bioRxiv*, 2021.01.26.428291 (2021).
48. L. Liu, *et al.*, The "two-brain" approach reveals the active role of task-deactivated default mode network in speech comprehension. *Cereb. Cortex* (2022) https:/doi.org/10.1093/cercor/bhab521.
49. M. Nguyen, *et al.*, Teacher–student neural coupling during teaching and learning. *Soc. Cogn. Affect. Neurosci.* **17**, 367–376 (2022).
50. G. J. Stephens, L. J. Silbert, U. Hasson, Speaker-listener neural coupling underlies successful communication. *Proc. Natl. Acad. Sci. U. S. A.* **107**, 14425–14430 (2010).
51. P. D. Antonenko, R. Davis, J. Wang, M. Celepkolu, On the Same Wavelength: Exploring Team Neurosynchrony in Undergraduate Dyads Solving a Cyberlearning

Problem With Collaborative Scripts. *Mind Brain Educ.* **13**, 4–13 (2019).

52. A. Zadbood, J. Chen, Y. C. Leong, K. A. Norman, U. Hasson, How we transmit memories to other brains: constructing shared neural representations via communication. *Cereb. Cortex* **27**, 4988–5000 (2017).
53. L. J. Silbert, C. J. Honey, E. Simony, D. Poeppel, U. Hasson, Coupled neural systems underlie the production and comprehension of naturalistic narrative speech. *Proc. Natl. Acad. Sci. U. S. A.* **111**, E4687–E4696 (2014).
54. L. S. Hamilton, A. G. Huth, The revolution will not be controlled: natural stimuli in speech neuroscience. *Lang. Cogn. Neurosci.* **35**, 573–582 (2020).
55. H. Lee, B. Bellana, J. Chen, What can narratives tell us about the neural bases of human memory? *Curr. Opin. Behav. Sci.* **32**, 111–119 (2020).
56. S. Sonkusare, M. Breakspear, C. Guo, Naturalistic stimuli in neuroscience: Critically acclaimed. *Trends Cogn. Sci.* **23**, 699–714 (2019).
57. S. A. Nastase, *et al.*, The “Narratives” fMRI dataset for evaluating models of naturalistic language comprehension. *Sci. Data* **8**, 250–250 (2021).
58. C. H. C. Chang, C. Lazaridi, Y. Yeshurun, K. A. Norman, U. Hasson, Relating the past with the present: Information integration and segregation during ongoing narrative processing. *J. Cogn. Neurosci.* **33**, 1106–1128 (2021).
59. Y. Benjamini, Y. Hochberg, Controlling the False Discovery Rate: A Practical and Powerful Approach to Multiple Testing. *J. R. Stat. Soc. Ser. B Methodol.* **57** (1995).
60. W. Penny, K. Friston, J. Ashburner, S. Kiebel, T. Nichols, *Statistical parametric mapping: The analysis of functional brain images* (2007) https:/doi.org/10.1016/B978-0-12-372560-8.X5000-1.

# Supplementary Information for

# Narrative construction drives a gradient of response lags across the cortical timescales hierarchy

Claire H. C. Chang1,*, Samuel A. Nastase1,*, and Uri Hasson1

1. Princeton Neuroscience Institute, Princeton University, Princeton, New Jersey, 08540, USA.

* To whom correspondence should be addressed:

Claire H. C. Chang, claire.hc.chang@gmail.com

Samuel A. Nastase, sam.nastase@gmail.com

**This PDF file includes:**

Figures S1 to S15

Tables S1

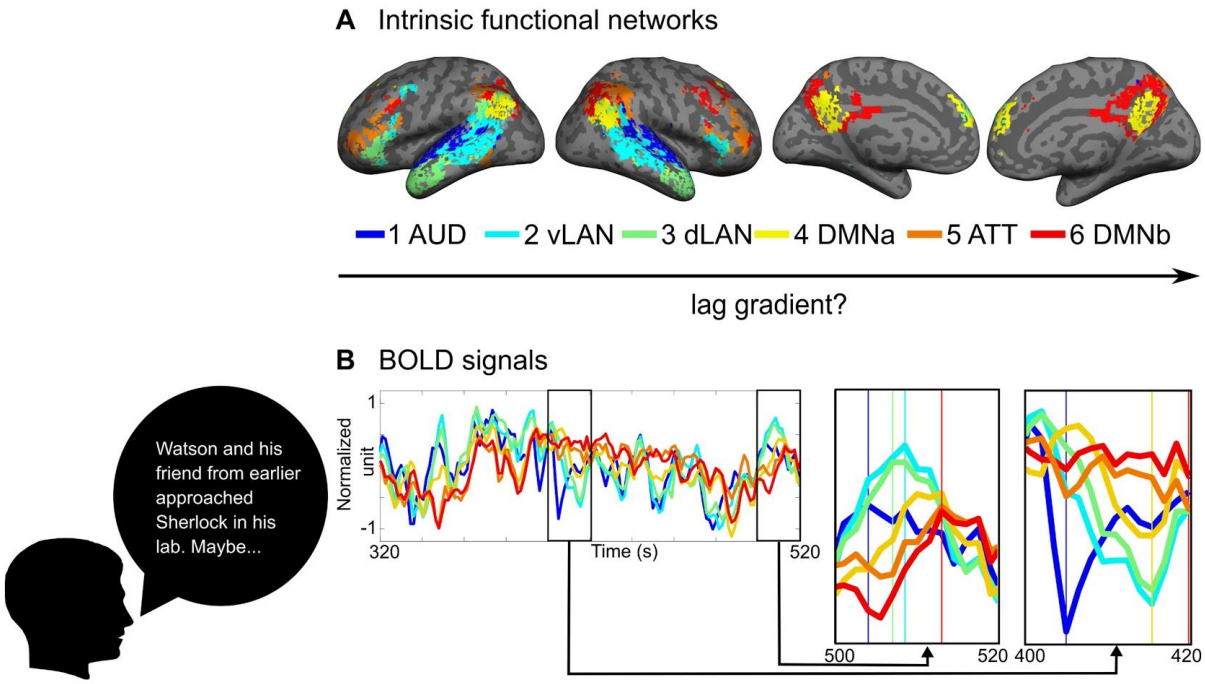


774

775 Fig. S1. Averaged fMRI response time series for six intrinsic functional networks while
776 subjects listened to a spoken story. (A) Functional networks defined by applying k-
777 means clustering to WSFC measured during rest and labeled based on anatomical
778 correspondence with previously defined functional regions following (25) (AUD:
779 auditory; vLAN: ventral language; dLAN: dorsal language; DMN: default mode network;
780 ATT: attention network). (B) Averaged fMRI responses time series in the “Sherlock”
781 dataset, extracted from the predefined network masks. Two example segments of the
782 response time series are highlighted at the bottom right. The peaks of the fluctuations in
783 a given window are indicated by colored vertical lines. Note the stereotyped lag in both
784 positive and negative BOLD fluctuations across networks; e.g. signal deflections in the
785 dark blue auditory network tend to precede deflections in the cyan/green language
786 networks, which tend to precede deflections in the yellow/red default mode networks.

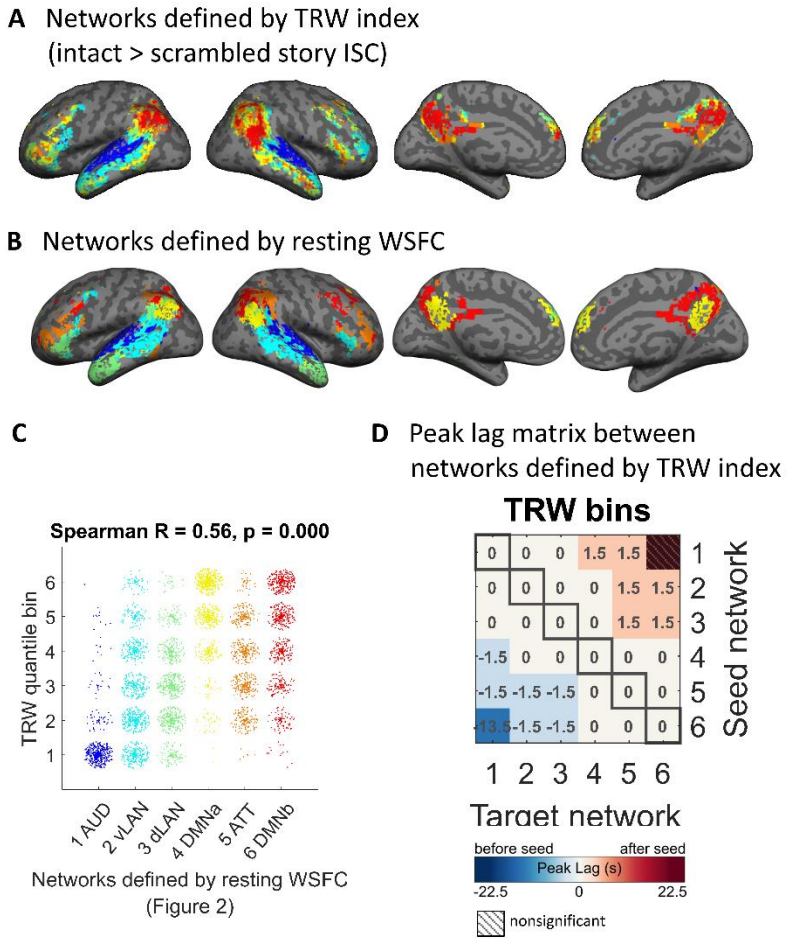


787

788 Fig. S2. Lag gradient between networks defined by TRW indices. (A) Networks
789 generated by splitting the TRW indices (intact > scrambled story ISC) into 6 bins by five
790 quantiles. (B) networks defined by applying k-mean clustering to resting WSFC (SI
791 Appendix, Fig. S1). (C) Networks defined by TRW index show a similar topographic
792 gradient as the networks defined by resting-state WSFC, from the auditory areas to
793 DMN, which is manifested by the significant correlation between the two sets of
794 networks index. Random jitters are added to better show the overlapped data points.
795 (D) Peak lag matrix between networks defined by TRW index across seven stories ($p$
796 < .05, FDR corrected). “Pie Man” was excluded from this analysis since it was used to
797 compute the TRW index.

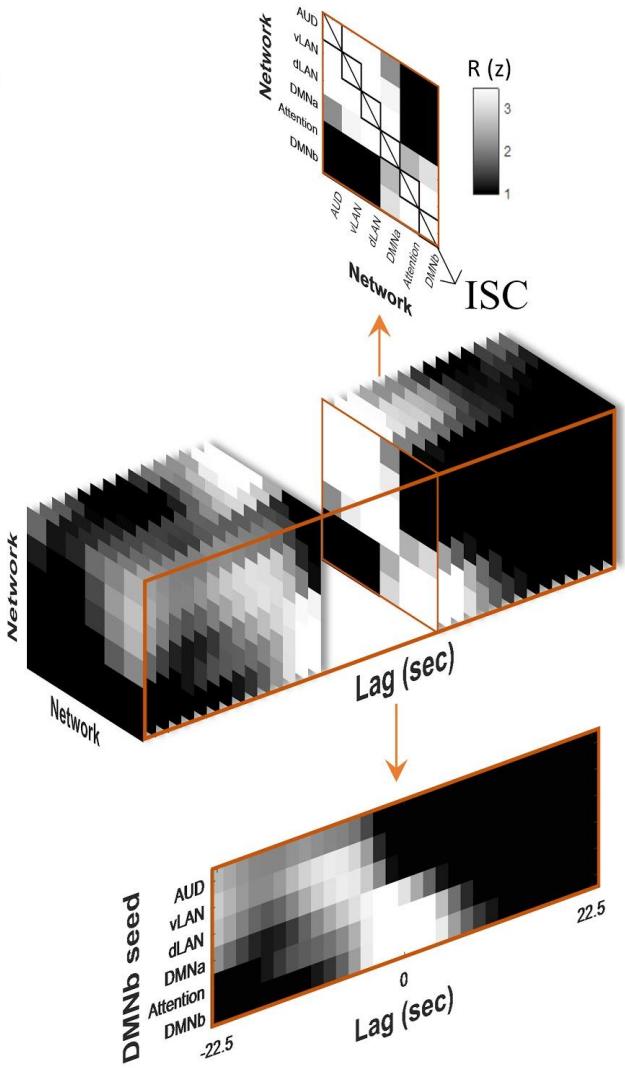


798

799

800 Fig. S3. The relationship between inter-subject functional connectivity (ISFC), inter-

801 subject-correlation (ISC), and lag-ISFC. This figure shows real data from the “Sherlock"

802 story.

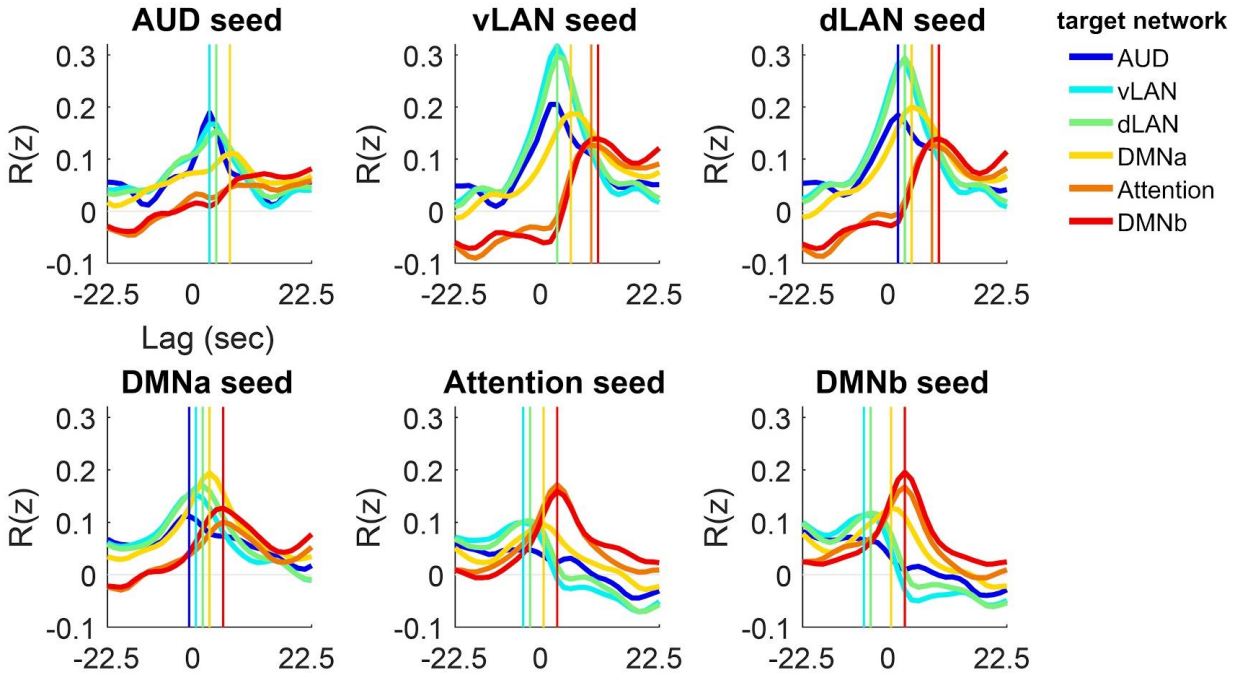


803

804 Fig. S4. Lag-ISFC curves between the six functional networks, corresponding to the left

805 panel of Fig. 3A. Fisher's z transformation was applied to the R-values before

806 averaging. Vertical lines indicate significant R peaks ($p < .05$, FDR correction).

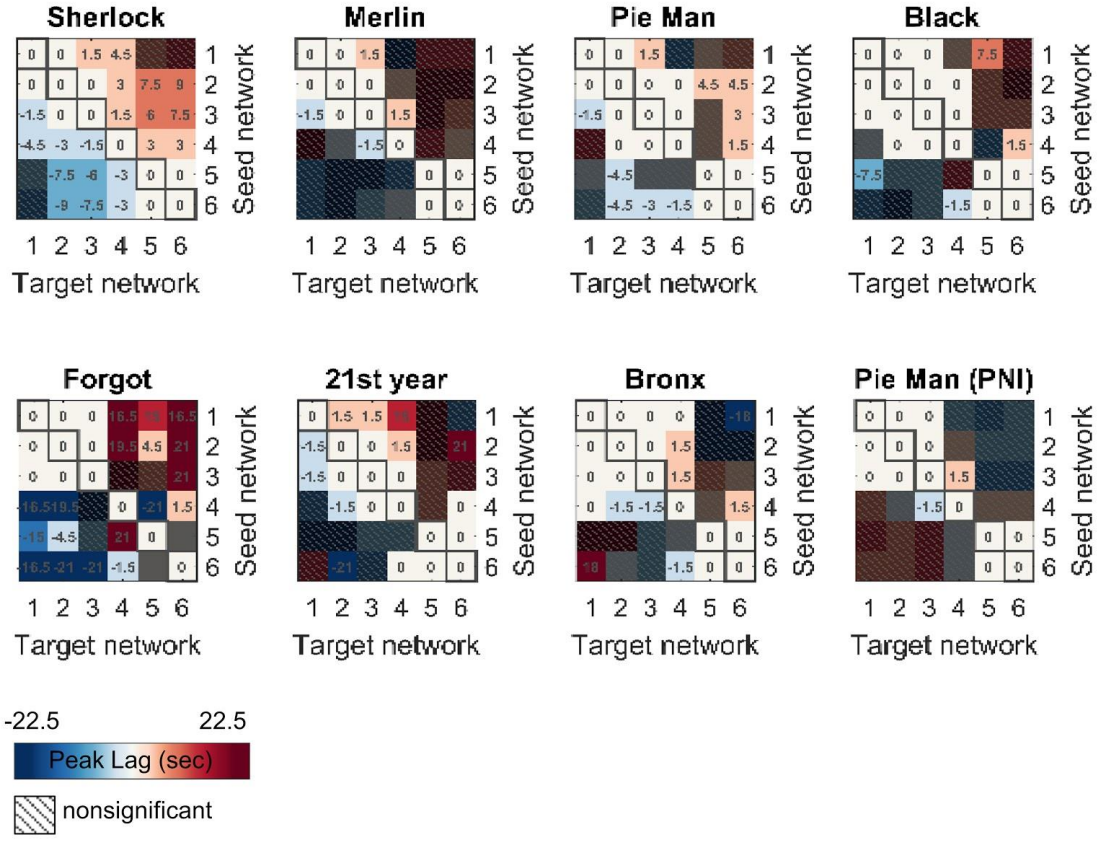


807

808 Fig. S5. The network × network peak lag matrix based on the lag-ISFC in each

809 individual story ($p < .05$, FDR corrected).

810

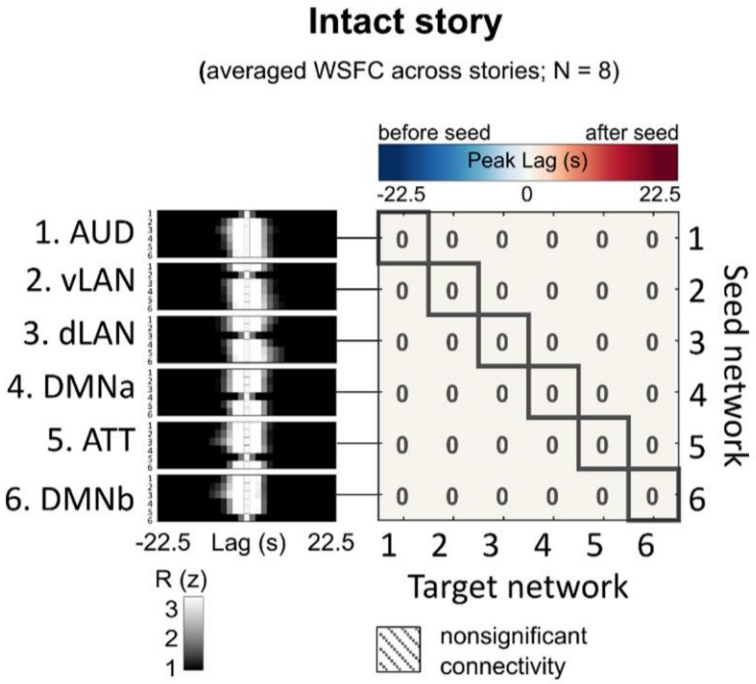


811

812 Fig. S6. The network × network peak lag matrix based on the averaged lag-WSFC

813 across eight stories ($p < .05$, FDR corrected).

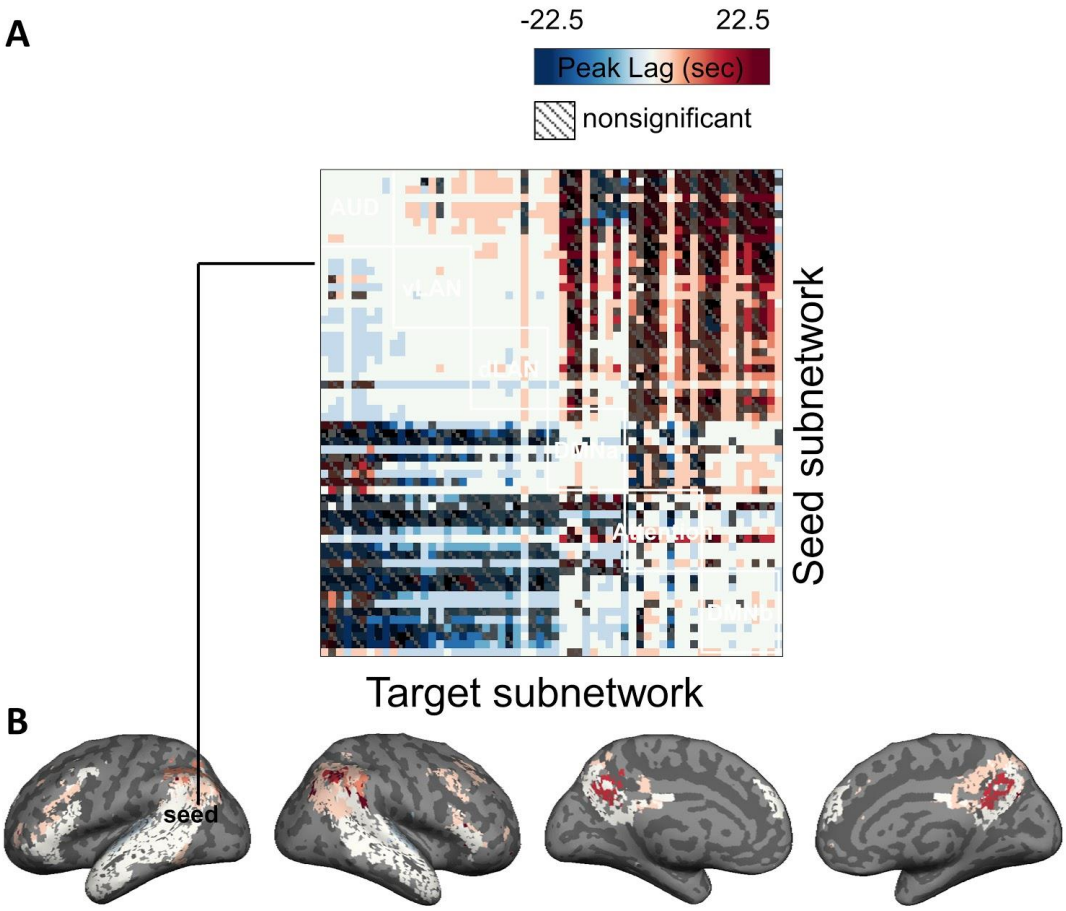


814

815 Fig. S7. Subnetwork × subnetwork peak lags based on the averaged lag-ISFC across
816 eight stories ($p < .05$, FDR corrected). The subnetworks were created by dividing each
817 of the six main functional networks (SI Appendix, Fig. S1) into 10 subnetworks, applying
818 k-means clustering to resting-state WSFC (k = 10 within each network). (A) The peak
819 lag matrix. (B) The brain map of significant peak lags between one seed subnetwork
820 (posterior superior/middle temporal gyrus) and all the sixty subnetworks.

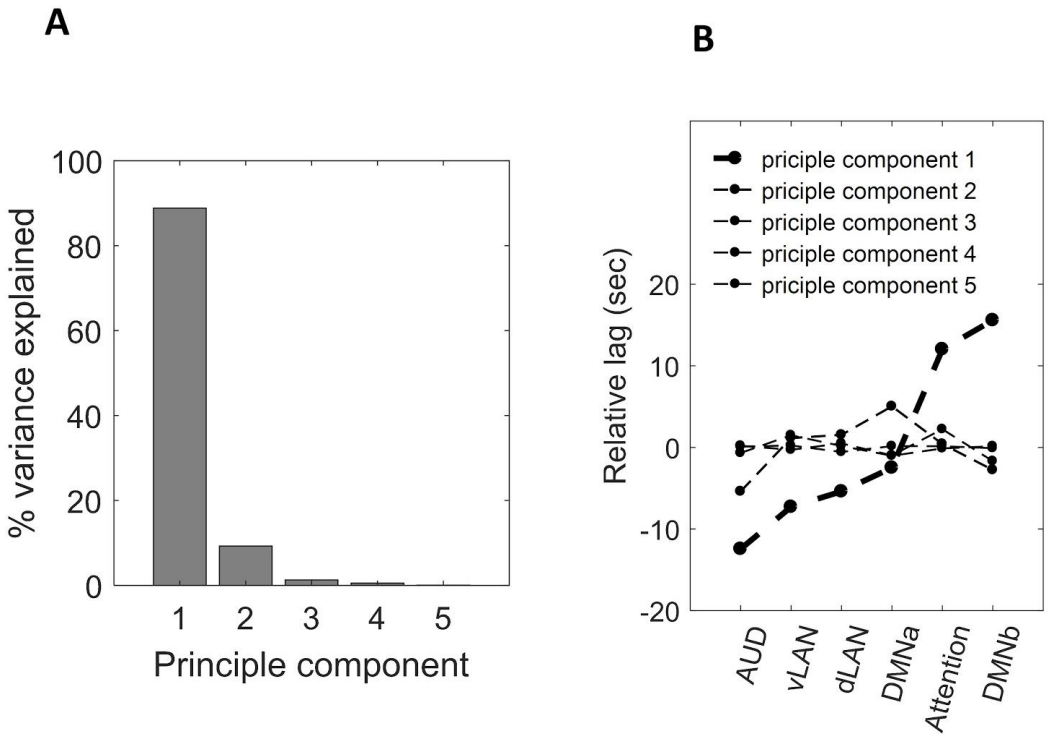


821

822 Fig. S8. Principal component analysis of the inter-network lag matrix across eight
823 stories (Fig. 3A). (A) The percentage of variance explained by each principal
824 component. (B) Relative-lag values from each principal component. Line thickness
825 indicates the percentage of variance explained by that component.

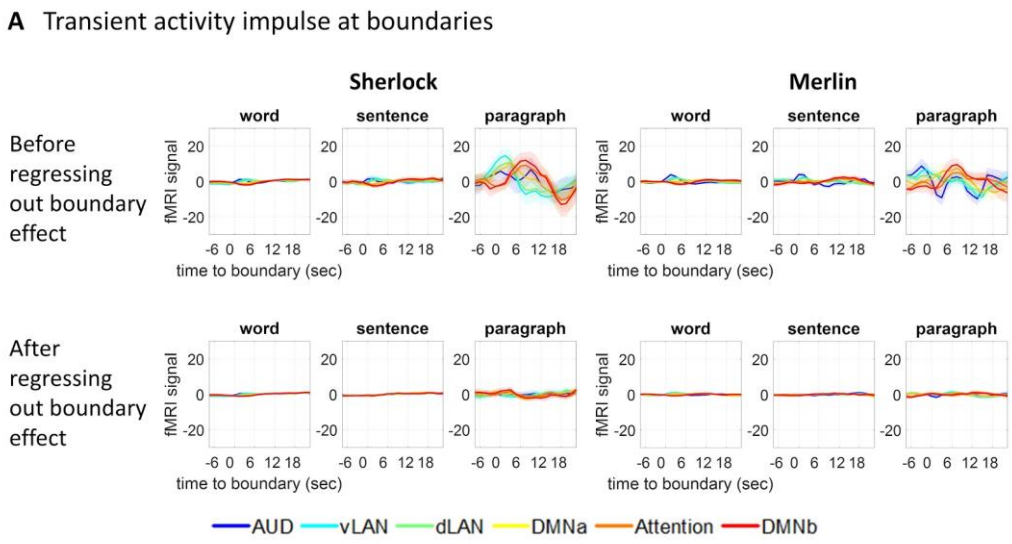


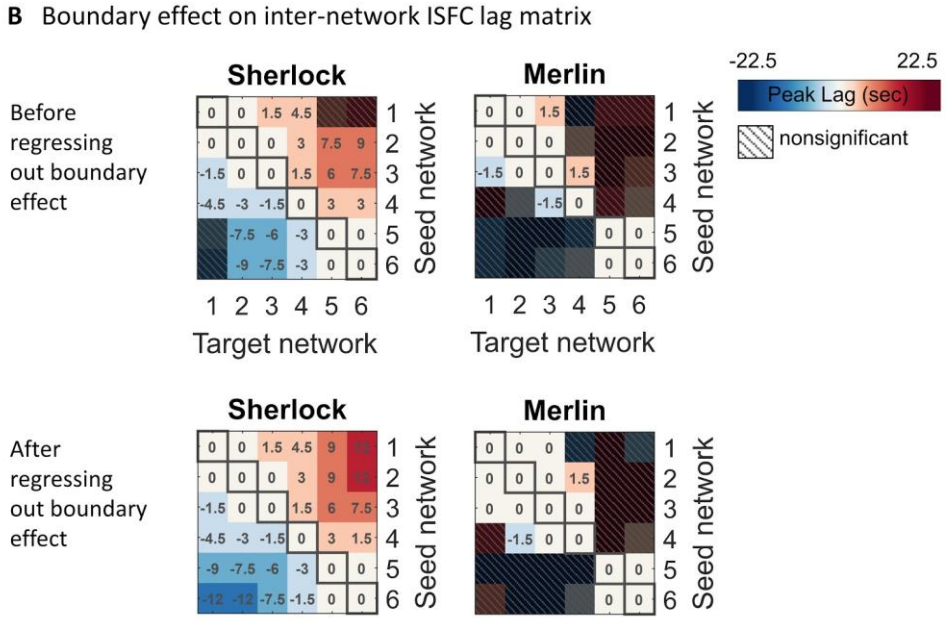


826

827 Fig. S9. Boundary effect on the network x network peak lag matrix across stories. (A)
828 The fMRI signals around word, sentence, and paragraph boundaries before and after
829 regressing out the boundary effects. Shaded areas indicate 95% confidence intervals
830 across subjects. (B) The peak lag matrix before and after regressing out the boundary
831 effects ($p < .05$, FDR corrected).

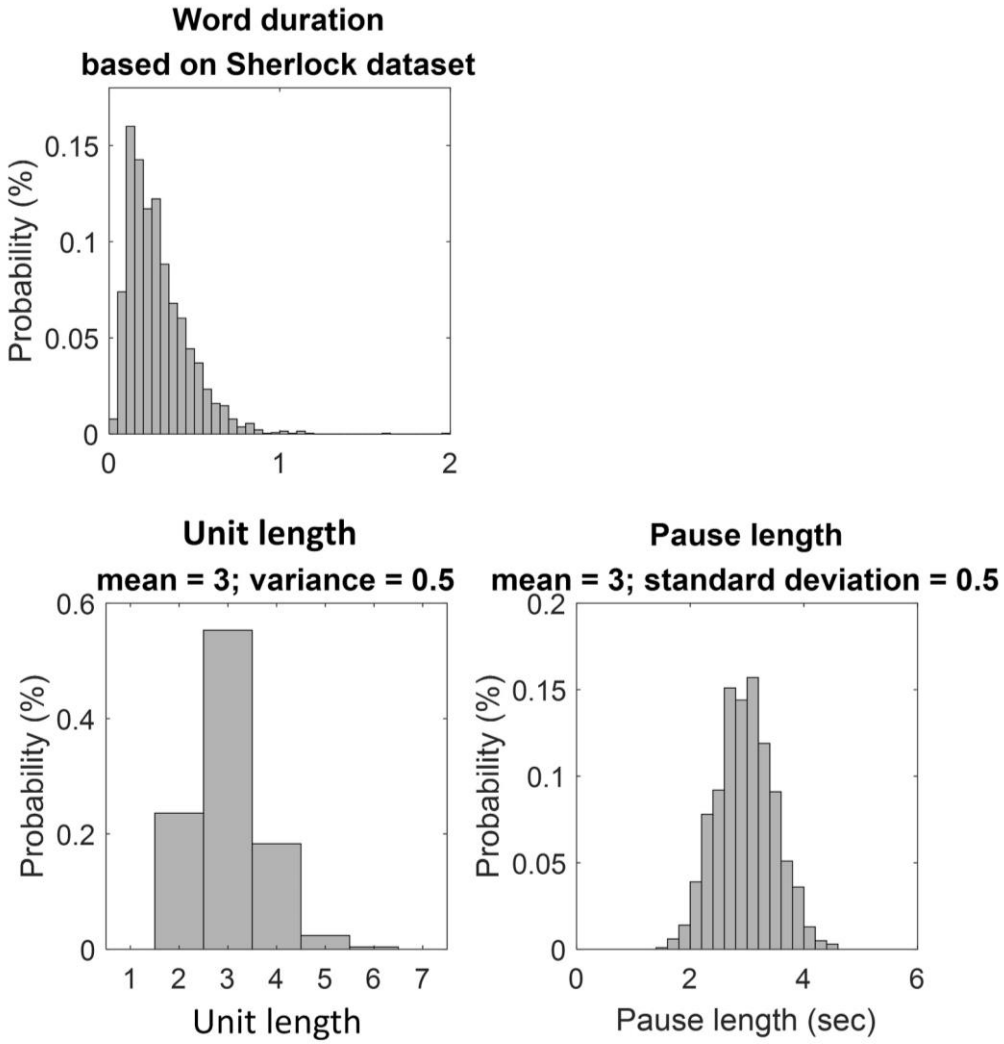


832

833 Fig. S10. The distributions of word duration, unit length, and pause length with the

834 simulation parameters described in Table S1.

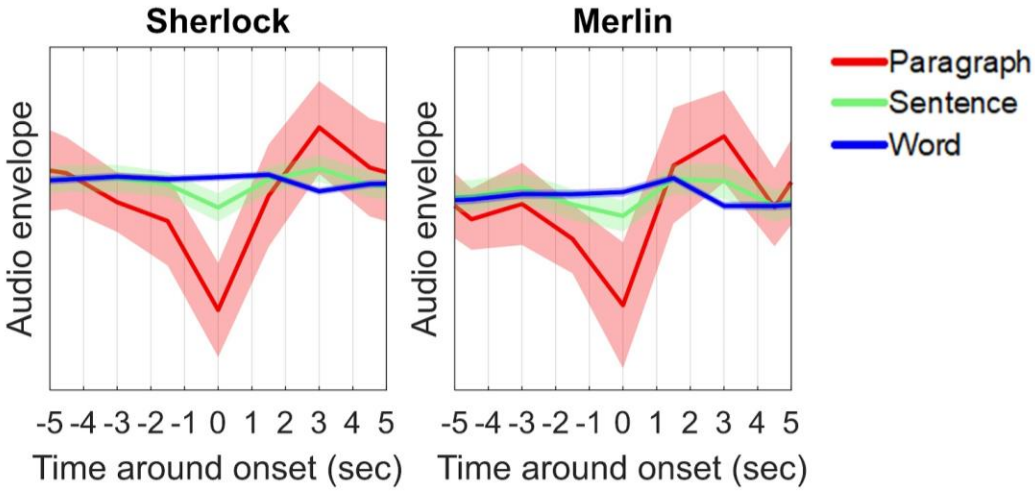


835

836 Fig. S11. The silent pause between paragraphs shown in real spoken stories. Shaded

837 areas indicate 95% confidence intervals.

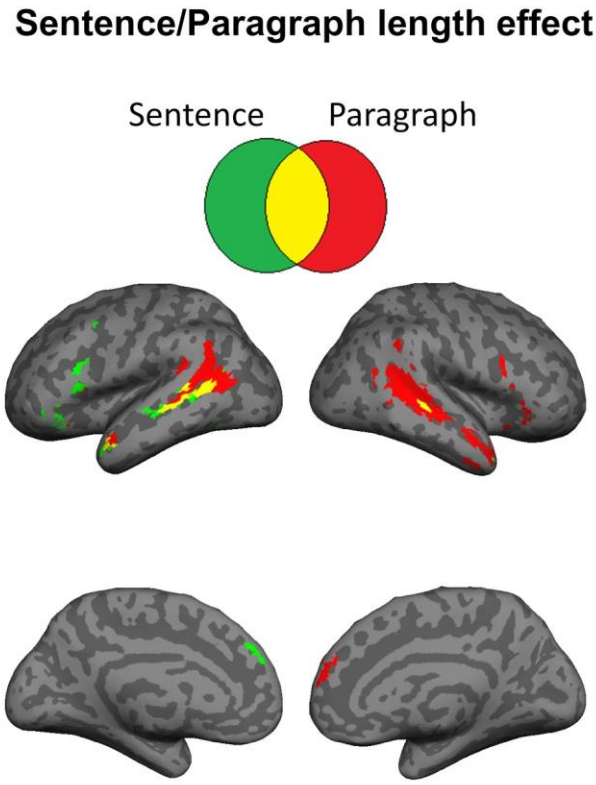


838

839 Fig. S12. Sentence and paragraph length effects in two time-stamped stories

840 ("Sherlock" & "Merlin") ($p < .005$, uncorrected). Significant length effect indicates

841 activation accumulation from the start toward the end of sentences or paragraphs.

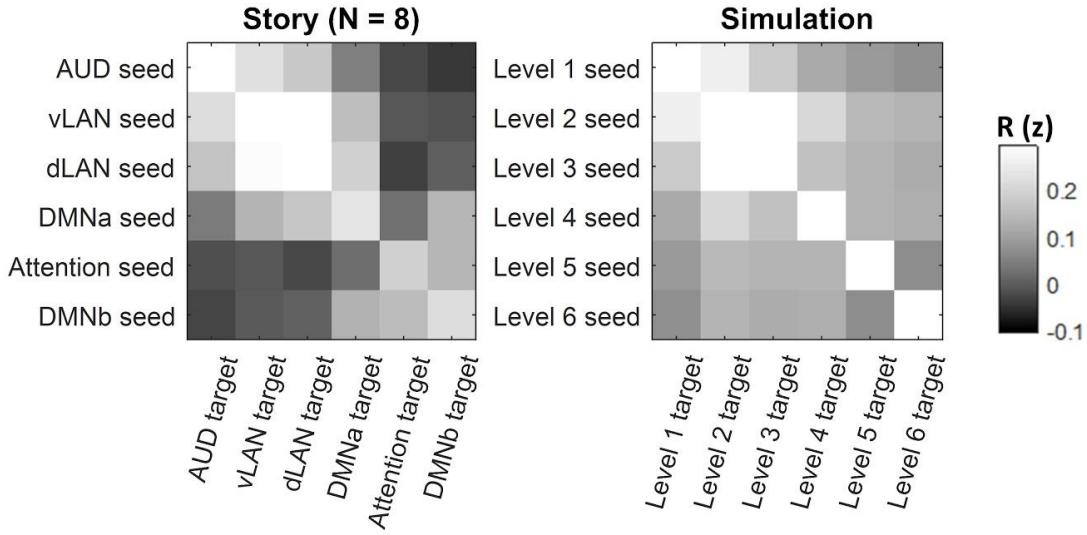


842

843 Fig. S13. ISFC matrices at lag 0 in real and simulated stories (the same simulation

844 parameters as in Table S1).

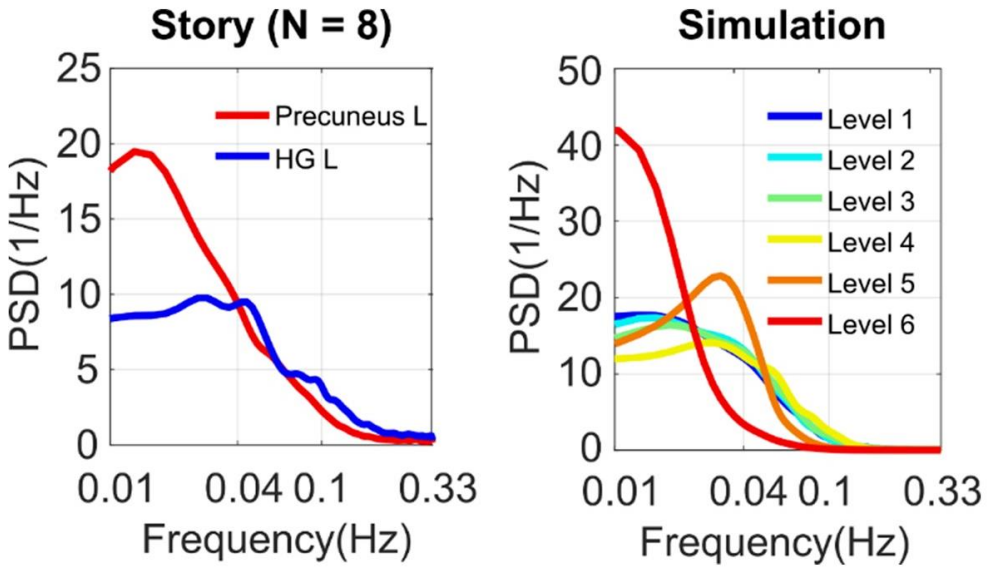


845

846 Fig. S14. Power spectral densities of real (left) and simulated (right, the same
847 parameter set as Table S1) BOLD responses to stories. PSD of the actual BOLD data
848 exhibited stronger low-frequency fluctuations at regions with longer temporal receptive
849 windows. Simulated BOLD responses show a similar pattern.

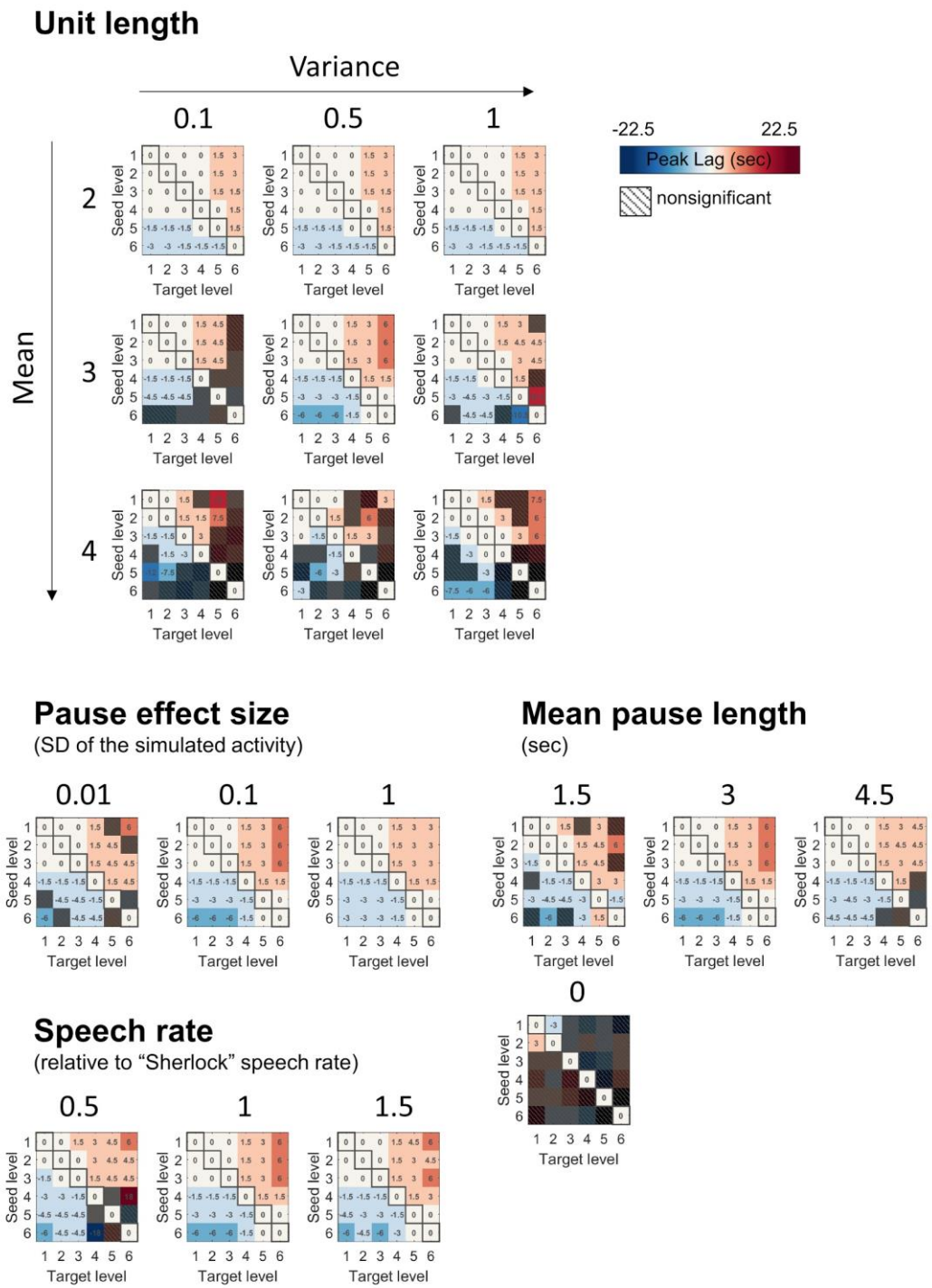


850

851 Fig. S15. Robust lag gradient within the parameter space bound by natural speech (the

852 same parameters as in Table S1 unless otherwise indicated) ($p < .05$, FDR correction).

853 Table S1. A set of exemplar stimulation parameters motivated by a spoken story

854 ("Sherlock"). SD: standard deviation.

| **Exemplar simulation parameters** | |
|---|---|
| speech rate (relative to "Sherlock") | 1 |
| mean unit length | 3 |
| unit length variance | 0.5 |
| temporal integration function | linearly increasing |
| mean pause length | 3 sec |
| pause length effect size<br>(in SD of the simulated activity) | 0.1 |

855